

Spectral and modal formulations for the Doppler-shifted field scattered by an object moving in a stratified medium

Yi-san Lai and Nicholas C. Makris^{a)}

Massachusetts Institute of Technology, Cambridge, Massachusetts 02139

(Received 5 April 2001; revised 13 March 2002; accepted 12 June 2002)

Spectral and normal mode formulations for the three-dimensional field scattered by an object moving in a stratified medium are derived using full-field wave theory. The derivations are based on Green's theorem for the time-domain scalar wave equation and account for Doppler effects induced by target motion as well as source and receiver motion. The formulations are valid when multiple scattering between the object and waveguide boundaries can be neglected, and the scattered field can be expressed as a linear function of the object's plane wave scattering function. The advantage of the spectral formulation is that it incorporates the entire wave number spectrum, including evanescent waves, and therefore can potentially be used at much closer ranges to the target than the modal formulation. The normal mode formulation is more computationally efficient but is limited to longer ranges. For a monochromatic source that excites N incident modes in the waveguide, there will be roughly N^2 distinct harmonic components in the scattered field. The Doppler shifts in the scattered field are highly dependent upon the waveguide environment, target shape, and measurement geometry. The Doppler effects are illustrated through a number of canonical examples. © 2003 Acoustical Society of America. [DOI: 10.1121/1.1499135]

PACS numbers: 43.30.Gv, 43.30.Vh, 43.30.Es [DLB]

I. INTRODUCTION

Standard active sonar and radar systems estimate the instantaneous velocity of a moving target in free space by resolving Doppler shifts in the frequency spectrum of scattered waves. To obtain all components of the velocity vector, a multistatic measurement geometry may be necessary. This type of active scenario is well suited to the velocity estimation of a distant body because the frequency spectrum of the source is known and controllable and so can be tailored to the resolution constraints of the problem at hand. In passive sonar and radar, however, velocity estimation by Doppler shift analysis is often less reliable because the distant object must itself radiate enough power to be detected. Additionally, the frequency spectrum of this radiation must be known, and have sufficiently narrow bandwidth and stability for Doppler shifts to be extracted robustly.

The problem of using active sonar to estimate the velocity of an underwater target moving in an ocean waveguide has complications not found in the free-space analogue. This is because propagation and scattering effects in a waveguide are typically not separable as they are in the far field free-space scenario. Also, multiple frequency components are typically present in the field scattered from an object moving in an ocean waveguide even if the active source of radiation is harmonic. An accurate physical model for the field scattered from an object moving in a stratified ocean waveguide must then be derived before techniques can be developed to estimate the submerged object's velocity. It is the goal of this paper to derive such a model and to investigate the Doppler effects induced by motion of a source, target, and receiver in a stratified ocean waveguide. Inclusion of source and re-

ceiver motion is also necessary because the source and receivers are typically mounted on research vessels that move with speeds similar to that of the target, and so induce their own Doppler effects that must be differentiated from those induced by the target.

Doppler effects induced by the motion of a radiating source that is passively measured at a moving receiver in free space have been extensively studied in acoustics.^{1,2} Doppler effects for the corresponding passive problem of a moving source and a moving receiver submerged in a stratified ocean waveguide have also been studied in the literature.^{3,4} Multimodal propagation and dispersion make the Doppler effects far more complicated in a waveguide than in free space. For example, the field radiated by a time harmonic source moving in an ocean waveguide can be received with multiple frequency components because of multimodal propagation.

A number of models exist for three-dimensional scattering from targets submerged in a stratified medium, as described in Ref. 5. A particularly convenient and widely used approach is the single-scatter theory developed in Refs. 5–8. The major advantage of this approach is that the scattered field is expressed in terms of the target's free-space plane wave scattering function. This theory is valid when (1) the propagation medium is horizontally stratified and range-independent; (2) the object is contained within an isovelocity layer; (3) multiple scattering between the object and waveguide boundaries make negligible contribution at the receiver; and (4) the range from the object to source and receiver is sufficiently large that the scattered field can be expressed as a linear function of the object's plane wave scattering function. This theory, however, assumes that the source, receiver, and target are not moving so that Doppler effects must be negligible.

In this paper, the single scatter theory is generalized to

^{a)}Electronic mail: makris@mit.edu

include the effects of source, receiver, and target motion. Analytical expressions are obtained for the field scattered to a moving receiver from a moving target in a stratified ocean waveguide by a moving source. The formulations are fully bistatic, and all the motions are assumed to be horizontal with constant velocities. Both the expressions for a simple harmonic source and a source with arbitrary time dependence are derived in this paper. Spectral and modal representations of the scattered field are derived from first principles using the time-domain formulation of Green's theorem. The spectral representation makes fewer assumptions and is more accurate than the normal mode representation at closer ranges, but the normal mode formulation provides a compelling physical interpretation and can be used at longer ranges without significant loss of accuracy. The single scatter theory of Refs. 6 and 7 then becomes a special case of the present more general theory when the source, receiver, and target are at rest. The four listed restrictions of the stationary single scatter theory also apply to the generalized theory developed in this paper.

It is noteworthy that when the target, source, or receiver are moving, the scattered field no longer obeys reciprocity, as is evident in our present formulation. The concept of a time-reversal mirror⁹⁻¹¹ therefore is not directly applicable under motion of the target, source, or receiver. This is true in both free space and in a stratified medium.

A simple and intuitive technique for deriving the field radiated from a moving source measured at a moving receiver using delta functions is also presented for both spectral and modal formulations. The spectral representation is identical to the result of Ref. 4. The normal mode representation makes more accurate approximations than those used in Ref. 3. The resulting expressions are used in the scattering problem to describe the incident field from the moving source at the moving target.

II. ANALYTIC FORMULATION

Analytical expressions for the field scattered from a moving source by a moving object measured at a moving receiver are derived from first principles using the time-domain scalar wave equation and the corresponding time-domain formulation of Green's theorem.

Some of the basic approximations and techniques used in Refs. 6 and 7 to solve the stationary scattering problem are also applied here. The major difference, however, is that we must solve the problem with the time-domain scalar wave equation instead of the Helmholtz equation to account for motion of the source, receiver, and target.

The time-domain scalar wave equation for the total field Φ_T with a source function $q(\mathbf{r}_0, t_0)$ is

$$\nabla_0^2 \Phi_T(\mathbf{r}_0, t_0) - \frac{1}{c^2} \frac{\partial^2 \Phi_T(\mathbf{r}_0, t_0)}{\partial t_0^2} = -q(\mathbf{r}_0, t_0). \quad (1)$$

The Green function for the time-domain scalar wave equation satisfies

$$\nabla_0^2 G(\mathbf{r}, t | \mathbf{r}_0, t_0) - \frac{1}{c^2} \frac{\partial^2 G(\mathbf{r}, t | \mathbf{r}_0, t_0)}{\partial t_0^2} = -\delta(\mathbf{r} - \mathbf{r}_0) \delta(t - t_0). \quad (2)$$

By applying Green's theorem, the total field Φ_T can be expressed as¹²

$$\begin{aligned} \Phi_T(\mathbf{r}, t) = & \int_0^{t^+} dt_0 \int dV_0 G(\mathbf{r}, t | \mathbf{r}_0, t_0) q(\mathbf{r}_0, t_0) \\ & + \int_0^{t^+} dt_0 \oint d\mathbf{S}_0 \cdot \left(G(\mathbf{r}, t | \mathbf{r}_0, t_0) \nabla_0 \Phi_T \right. \\ & \left. - \Phi_T \nabla_0 G(\mathbf{r}, t | \mathbf{r}_0, t_0) \right) \\ & - \frac{1}{c^2} \int dV_0 \left[\frac{\partial G(\mathbf{r}, t | \mathbf{r}_0, t_0)}{\partial t_0} \Phi_T \right. \\ & \left. - G(\mathbf{r}, t | \mathbf{r}_0, t_0) \frac{\partial \Phi_T}{\partial t_0} \right]_{t_0=0}, \end{aligned} \quad (3)$$

which differs from Eq. (7.3.5) of Ref. 12 only by a 4π factor due to differing choices for the delta function normalization. The first integral represents the incident field Φ_i induced by the source, and the second integral represents the scattered field Φ_s . The third integral accounts for the transient response. For example, given a time harmonic source turned on at $t_0=0$, this integral vanishes after the source has been operating for a time duration t^+ large compared to the source period. The first two integrals then represent the steady state response, and the total field is the summation of the first two integrals

$$\Phi_T(\mathbf{r}, t) = \Phi_i(\mathbf{r}, t) + \Phi_s(\mathbf{r}, t) \quad (4)$$

with incident field

$$\Phi_i(\mathbf{r}, t) = \int_0^{t^+} dt_0 \int dV_0 G(\mathbf{r}, t | \mathbf{r}_0, t_0) q(\mathbf{r}_0, t_0) \quad (5)$$

and scattered field

$$\begin{aligned} \Phi_s(\mathbf{r}, t) = & \int_0^{t^+} dt_0 \oint d\mathbf{S}_0 \cdot \left(G(\mathbf{r}, t | \mathbf{r}_0, t_0) \nabla_0 \Phi_T \right. \\ & \left. - \Phi_T \nabla_0 G(\mathbf{r}, t | \mathbf{r}_0, t_0) \right). \end{aligned} \quad (6)$$

Following the type of abbreviating convention adopted in Refs. 6 and 7, we will drop the first term in Eq. (6) in the derivation to avoid cumbersome and uninformative algebra. The derivation with both terms proceeds in exactly the same manner and leads to exactly the same expression for the scattered field. This expression is in terms of the object's plane wave scattering function for an object with arbitrary boundary conditions.⁵⁻⁷

The scattered field from a rigid surface with unspecified shape is

$$\begin{aligned} \Phi_s(\mathbf{r}, t) = & - \int_0^{t^+} dt_0 \oint d\mathbf{S}_0 \cdot \left(\Phi_T(\mathbf{r}_0, t_0) \nabla_0 G(\mathbf{r}, t | \mathbf{r}_0, t_0) \right) \\ = & - \int_0^{t^+} dt_0 \oint d\mathbf{S}_0 \cdot \left([\Phi_i(\mathbf{r}_0, t_0) \right. \\ & \left. + \Phi_s(\mathbf{r}_0, t_0)] \nabla_0 G(\mathbf{r}, t | \mathbf{r}_0, t_0) \right). \end{aligned} \quad (7)$$

For a steady wave problem, this leads to Eq. (37) of Ref. 6 directly.

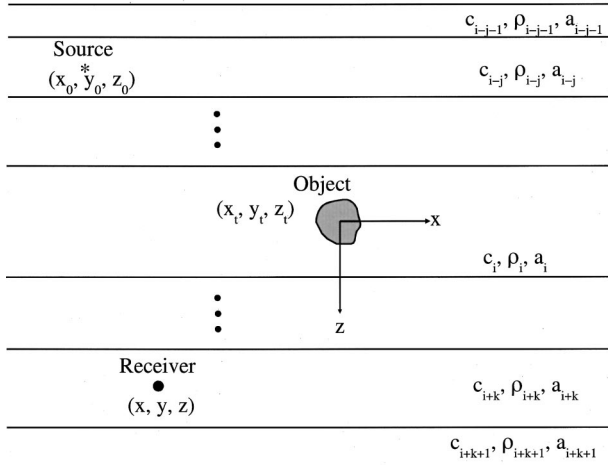


FIG. 1. Measurement geometry for a submerged object in a horizontally stratified waveguide ensounded by a point source. The coordinate system is centered at the centroid of the object with positive z pointing down. Each layer i is characterized by sound speed c_i , density ρ_i , and attenuation a_i .

For economy, the notation of Ref. 7 is used here and in the remainder of this article. Figure 2 of Ref. 7 shows the geometry of spatial and wave number coordinates. For example, the object centroid *at the initial location of the object* is at the center of all coordinate systems, as shown in Fig. 1. Source coordinates are denoted by (x_0, y_0, z_0) , receiver coordinates by (x, y, z) , and coordinates on the surface of the target by $(x_\sigma, y_\sigma, z_\sigma)$ where the positive z axis points downward and is normal to the interfaces between horizontal strata. Spatial cylindrical (ρ, θ, z) and spherical (r, θ, ϕ) systems are defined by $x = r \sin \theta \cos \phi$, $y = r \sin \theta \sin \phi$, $z = r \cos \theta$, and $\rho^2 = x^2 + y^2$. Wave number coordinates for the incident $(\xi_{ix}, \xi_{iy}, \gamma_i)$ and scattered field (ξ_x, ξ_y, γ) also originate at the target center and are related to polar and azimuthal propagation angles by $\xi^2 = \xi_x^2 + \xi_y^2$, where

$$\xi_x = k \sin \alpha \cos \beta, \quad (8)$$

$$\xi_y = k \sin \alpha \sin \beta, \quad (9)$$

$$\xi_z = k \cos \alpha, \quad (10)$$

$$k^2 = \left(\frac{\omega}{c}\right)^2 = \gamma^2 + \xi^2. \quad (11)$$

The superscript 0 is used to denote the initial positions of the source, target, and receiver, for example, $x(t)|_{t=0} = x^0$.

A. Spectral representation of the Doppler-shifted field scattered from a moving target by a simple-harmonic source in a stratified waveguide

A spectral representation for the field from a moving source, scattered by a moving target at a moving receiver, is now derived. The source is taken to be a simple-harmonic one with frequency Ω , and the motions of the source, target, and receiver are all horizontal with constant velocity.

In order to calculate the scattered field, Eq. (7) is applied where the incident field at a point \mathbf{r}_σ on the surface of the target depends on time t_σ . The scattered field at the receiver location \mathbf{r} at time t can then be calculated by

$$\Phi_s(\mathbf{r}, t) = - \int_0^{t^+} dt_\sigma \oint d\mathbf{S}_\sigma \cdot \left([\Phi_i(\mathbf{r}_\sigma, t_\sigma) + \Phi_s(\mathbf{r}_\sigma, t_\sigma)] \nabla_\sigma G(\mathbf{r}, t | \mathbf{r}_\sigma, t_\sigma) \right), \quad (12)$$

where the surface integral is carried out on the surface of the scatterer.

The incident field induced by a simple-harmonic source at frequency Ω moving with horizontal velocity \mathbf{v}_0 and received at a point \mathbf{r}_σ on the surface of an object moving with horizontal velocity \mathbf{v}_σ is obtained from Eq. (A10) as

$$\Phi_i(\mathbf{r}_\sigma, t) = \frac{1}{2\pi} \int_{-\infty}^{\infty} d^2 \xi_i g(z_\sigma, z_0; \Omega + \xi_i \cdot \mathbf{v}_0) \times e^{i \xi_i \cdot (\boldsymbol{\rho}_\sigma^0 - \boldsymbol{\rho}_0^0)} e^{-i(\Omega + \xi_i \cdot (\mathbf{v}_0 - \mathbf{v}_\sigma))t}. \quad (13)$$

With the decomposition proposed in Eq. (6) of Ref. 7, the depth-dependent Green function defined in Eq. (A7) becomes

$$g(z_\sigma, z_0; \omega_i) = A(z_0; \omega_i) e^{i \gamma_i(\omega_i) z_\sigma} + B(z_0; \omega_i) e^{-i \gamma_i(\omega_i) z_\sigma} \quad (14)$$

with the shifted frequency of the incident field

$$\omega_i = \Omega + \xi_i \cdot \mathbf{v}_0. \quad (15)$$

The location of a point on the surface of the target is

$$\mathbf{r}_\sigma = \mathbf{r}_\sigma^0 + \mathbf{v}_\sigma t_\sigma \quad (16)$$

with \mathbf{r}_σ^0 as its initial location at $t_\sigma = 0$ and \mathbf{v}_σ as its horizontal velocity. The incident field in Eq. (13) then becomes

$$\Phi_i(\mathbf{r}_\sigma, t_\sigma) = \frac{1}{2\pi} \int_{-\infty}^{\infty} d^2 \xi_i e^{-i \xi_i \cdot \boldsymbol{\rho}_\sigma^0} e^{-i(\Omega + \xi_i \cdot (\mathbf{v}_0 - \mathbf{v}_\sigma))t_\sigma} \times [A(z_0; \omega_i) e^{i(\xi_i \cdot \boldsymbol{\rho}_\sigma^0 + \gamma_i(\omega_i) z_\sigma)} + B(z_0; \omega_i) e^{i(\xi_i \cdot \boldsymbol{\rho}_\sigma^0 - \gamma_i(\omega_i) z_\sigma)}]. \quad (17)$$

The spectral representation of Green's function for the Helmholtz equation in a stratified waveguide is

$$G(\mathbf{r} | \mathbf{r}_\sigma; \omega) = \frac{1}{2\pi} \int_{-\infty}^{\infty} d^2 \xi g(z, z_\sigma; \omega) e^{i \xi \cdot (\boldsymbol{\rho} - \boldsymbol{\rho}_\sigma)}. \quad (18)$$

Similarly, the depth-dependent Green function in Eq. (18) is decomposed as

$$g(z, z_\sigma; \omega) = C(z; \omega) e^{i \gamma_i(\omega) z_\sigma} + D(z; \omega) e^{-i \gamma_i(\omega) z_\sigma}. \quad (19)$$

The motion of the receiver is expressed as

$$\mathbf{r} = \mathbf{r}^0 + \mathbf{v} t, \quad (20)$$

where \mathbf{r}^0 is its initial location at time $t=0$ and \mathbf{v} is its horizontal velocity. The Green function for the time-domain scalar wave equation from the surface of the target \mathbf{r}_σ at time t_σ to the receiver location \mathbf{r} at time t then becomes

$$G(\mathbf{r}, t | \mathbf{r}_\sigma, t_\sigma) = \frac{1}{2\pi} \int_{-\infty}^{\infty} d\omega e^{-i\omega(t-t_\sigma)} \frac{1}{2\pi} \int_{-\infty}^{\infty} d^2 \boldsymbol{\xi} e^{i\boldsymbol{\xi} \cdot \boldsymbol{\rho}^0} e^{i\boldsymbol{\xi} \cdot \mathbf{v} t} e^{-i\boldsymbol{\xi} \cdot \mathbf{v}_\sigma t_\sigma} \times [C(z; \omega) e^{i(-\boldsymbol{\xi} \cdot \boldsymbol{\rho}_\sigma^0 + \gamma_i(\omega) z_\sigma)} + D(z; \omega) e^{i(-\boldsymbol{\xi} \cdot \boldsymbol{\rho}_\sigma^0 - \gamma_i(\omega) z_\sigma)}]. \quad (21)$$

Inserting Eqs. (17) and (21) into Eq. (12) leads to the scattered field

$$\Phi_s(\mathbf{r}, t) = -\frac{1}{2\pi} \int_0^{t^+} dt_\sigma \oint d\mathbf{S}_\sigma \cdot \left\{ \left[\frac{1}{2\pi} \int_{-\infty}^{\infty} d^2 \boldsymbol{\xi}_i e^{-i\boldsymbol{\xi}_i \cdot \boldsymbol{\rho}_0^0} e^{-i(\Omega + \boldsymbol{\xi}_i \cdot (\mathbf{v}_0 - \mathbf{v}_\sigma)) t_\sigma} \times [A(z_0; \omega_i) e^{i(\boldsymbol{\xi}_i \cdot \boldsymbol{\rho}_\sigma^0 + \gamma_i(\omega_i) z_\sigma)} + B(z_0; \omega_i) e^{i(\boldsymbol{\xi}_i \cdot \boldsymbol{\rho}_\sigma^0 - \gamma_i(\omega_i) z_\sigma)}] + \Phi_s(\mathbf{r}_\sigma, t_\sigma) \right] \times \nabla_\sigma \left(\int_{-\infty}^{\infty} d\omega e^{-i\omega(t-t_\sigma)} \frac{1}{2\pi} \int_{-\infty}^{\infty} d^2 \boldsymbol{\xi} e^{i\boldsymbol{\xi} \cdot \boldsymbol{\rho}^0} e^{i\boldsymbol{\xi} \cdot \mathbf{v} t} e^{-i\boldsymbol{\xi} \cdot \mathbf{v}_\sigma t_\sigma} \times [C(z; \omega) e^{i(-\boldsymbol{\xi} \cdot \boldsymbol{\rho}_\sigma^0 + \gamma_i(\omega) z_\sigma)} + D(z; \omega) e^{i(-\boldsymbol{\xi} \cdot \boldsymbol{\rho}_\sigma^0 - \gamma_i(\omega) z_\sigma)}] \right) \right\}, \quad (22)$$

where $\boldsymbol{\xi} \cdot \boldsymbol{\rho} + \gamma z = kr \eta(\alpha, \beta; \theta, \phi)$ and

$$\eta(\alpha, \beta; \theta, \phi) = \cos \alpha \cos \theta + \sin \alpha \sin \theta \cos(\beta - \phi) \quad (23)$$

is the cosine of the angle between the propagation direction (α, β) and field coordinate direction (θ, ϕ) where the angles α, β may be complex. Substituting this angular representation into Eq. (22) yields

$$\Phi_s(\mathbf{r}, t) = -\frac{1}{2\pi} \int_0^{t^+} dt_\sigma \oint d\mathbf{S}_\sigma \cdot \left\{ \left[\frac{1}{2\pi} \int_{-\infty}^{\infty} d^2 \boldsymbol{\xi}_i e^{-i\boldsymbol{\xi}_i \cdot \boldsymbol{\rho}_0^0} e^{-i(\Omega + \boldsymbol{\xi}_i \cdot (\mathbf{v}_0 - \mathbf{v}_\sigma)) t_\sigma} \times [A(z_0; \omega_i) e^{ik(\omega_i) r_\sigma^0 \eta(\alpha_i(\omega_i), \beta_i; \theta_\sigma^0, \phi_\sigma^0)} + B(z_0; \omega_i) e^{ik(\omega_i) r_\sigma^0 \eta(\pi - \alpha_i(\omega_i), \beta_i; \theta_\sigma^0, \phi_\sigma^0)}] + \Phi_s(\mathbf{r}_\sigma, t_\sigma) \right] \times \nabla_\sigma \left(\int_{-\infty}^{\infty} d\omega e^{-i\omega(t-t_\sigma)} \frac{1}{2\pi} \int_{-\infty}^{\infty} d^2 \boldsymbol{\xi} e^{i\boldsymbol{\xi} \cdot \boldsymbol{\rho}^0} e^{i\boldsymbol{\xi} \cdot \mathbf{v} t} e^{-i\boldsymbol{\xi} \cdot \mathbf{v}_\sigma t_\sigma} \times [C(z; \omega) e^{-ik(\omega) r_\sigma^0 \eta(\pi - \alpha(\omega), \beta; \theta_\sigma^0, \phi_\sigma^0)} + D(z; \omega) e^{-ik(\omega) r_\sigma^0 \eta(\alpha(\omega), \beta; \theta_\sigma^0, \phi_\sigma^0)}] \right) \right\}, \quad (24)$$

where (α_i, β_i) is the propagation direction of the incident plane waves and $(\theta_\sigma^0, \phi_\sigma^0)$ is the direction of \mathbf{r}_σ^0 , the initial location of a point on the target with respect to the initial position of the target centroid which is the origin of all coordinates.

For low Mach number motion, the scattered field on the surface of the object in Eq. (24) is approximately

$$\hat{\Phi}_s(\mathbf{r}_\sigma, t_\sigma) \approx \hat{\Phi}_s(\mathbf{r}_\sigma; \omega_i) e^{-i\omega_i t_\sigma} \quad (25)$$

for a given incident plane wave. The wave number vectors for the downgoing and upgoing waves are defined as

$$\mathbf{k}_i^+ = \boldsymbol{\xi}_i + \gamma_i \hat{\mathbf{i}}_z, \quad (26)$$

$$\mathbf{k}_i^- = \boldsymbol{\xi}_i - \gamma_i \hat{\mathbf{i}}_z. \quad (27)$$

When the Mach number of the target motion is small, the scattered fields on the surface of the moving target $\hat{\Phi}_s(\mathbf{r}_\sigma, \mathbf{k}_i^+; \omega_i)$ and $\hat{\Phi}_s(\mathbf{r}_\sigma, \mathbf{k}_i^-; \omega_i)$, which are induced by downgoing and upgoing incident plane waves with unit amplitudes, can be approximated as the scattered fields at the initial locations of the target multiplied by a phase shift factor $e^{i\boldsymbol{\xi}_i \cdot \mathbf{v}_\sigma t_\sigma}$ that accounts for the *rigid body translation of the centroid*. The scattered field on the object then becomes

$$\Phi_s(\mathbf{r}_\sigma, t_\sigma) = \frac{1}{2\pi} \int_{-\infty}^{\infty} d^2 \boldsymbol{\xi}_i e^{-i\boldsymbol{\xi}_i \cdot \boldsymbol{\rho}_0^0} e^{-i(\Omega + \boldsymbol{\xi}_i \cdot (\mathbf{v}_0 - \mathbf{v}_\sigma)) t_\sigma} \times [A(z_0; \omega_i) \hat{\Phi}_s(\mathbf{r}_\sigma^0, \mathbf{k}_i^+; \omega_i) + B(z_0; \omega_i) \hat{\Phi}_s(\mathbf{r}_\sigma^0, \mathbf{k}_i^-; \omega_i)]. \quad (28)$$

Introducing Eq. (28) into Eq. (24), then leads to the scattered field

$$\begin{aligned}
\Phi_s(\mathbf{r}, t) = & -\frac{1}{2\pi} \int_0^{t^+} dt_\sigma \oint d\mathbf{S}_\sigma \cdot \left\{ \left[\frac{1}{2\pi} \int_{-\infty}^{\infty} d^2\xi e^{-i\xi_i \cdot \mathbf{r}_0^0} e^{-i(\Omega + \xi_i \cdot (\mathbf{v}_0 - \mathbf{v}_\sigma)) t_\sigma} \right. \right. \\
& \times (A(z_0; \omega_i) \{e^{ik(\omega_i) r_\sigma^0} \eta(\alpha_i(\omega_i), \beta_i; \theta_\sigma^0, \phi_\sigma^0) + \hat{\Phi}_s(\mathbf{r}_\sigma^0, \mathbf{k}_i^+; \omega_i)\} \\
& + B(z_0; \omega_i) \{e^{ik(\omega_i) r_\sigma^0} \eta(\pi - \alpha_i(\omega_i), \beta_i; \theta_\sigma^0, \phi_\sigma^0) + \hat{\Phi}_s(\mathbf{r}_\sigma^0, \mathbf{k}_i^-; \omega_i)\}) \left. \right] \\
& \times \nabla_\sigma \left(\int_{-\infty}^{\infty} d\omega e^{-i\omega(t-t_\sigma)} \frac{1}{2\pi} \int_{-\infty}^{\infty} d^2\xi e^{i\xi \cdot \mathbf{r}^0} e^{i\xi \cdot \mathbf{v} t} e^{-i\xi \cdot \mathbf{v}_\sigma t_\sigma} \right. \\
& \left. \left. \times [C(z; \omega) e^{-ik(\omega) r_\sigma^0} \eta(\pi - \alpha(\omega), \beta; \theta_\sigma^0, \phi_\sigma^0) + D(z; \omega) e^{-ik(\omega) r_\sigma^0} \eta(\alpha(\omega), \beta; \theta_\sigma^0, \phi_\sigma^0)] \right] \right\}. \tag{29}
\end{aligned}$$

For sufficiently long time duration t , the integral over t_σ introduces the delta function $\delta(\omega - \Omega - \xi_i \cdot (\mathbf{v}_0 - \mathbf{v}_\sigma) - \xi \cdot \mathbf{v}_\sigma)$ to the integrand. Integrating over ω then leads to

$$\begin{aligned}
\Phi_s(\mathbf{r}, t) = & -\frac{1}{2\pi} \int_{-\infty}^{\infty} d^2\xi \int_{-\infty}^{\infty} d^2\xi e^{i[\xi \cdot \mathbf{r}^0 - \xi_i \cdot \mathbf{r}_0^0]} e^{-i[\Omega + \xi_i \cdot (\mathbf{v}_0 - \mathbf{v}_\sigma) + \xi \cdot (\mathbf{v}_\sigma - \mathbf{v})] t} \\
& \times \oint d\mathbf{S}_\sigma \cdot \left\{ [A(z_0; \omega_i) \{e^{ik(\omega_i) r_\sigma^0} \eta(\alpha_i(\omega_i), \beta_i; \theta_\sigma^0, \phi_\sigma^0) + \hat{\Phi}_s(\mathbf{r}_\sigma^0, \mathbf{k}_i^+; \omega_i)\} \right. \\
& + B(z_0; \omega_i) \{e^{ik(\omega_i) r_\sigma^0} \eta(\pi - \alpha_i(\omega_i), \beta_i; \theta_\sigma^0, \phi_\sigma^0) + \hat{\Phi}_s(\mathbf{r}_\sigma^0, \mathbf{k}_i^-; \omega_i)\}] \\
& \left. \times \nabla_\sigma \left(C(z; \omega_s) e^{-ik(\omega_s) r_\sigma^0} \eta(\pi - \alpha(\omega_s), \beta; \theta_\sigma^0, \phi_\sigma^0) + D(z; \omega_s) e^{-ik(\omega_s) r_\sigma^0} \eta(\alpha(\omega_s), \beta; \theta_\sigma^0, \phi_\sigma^0) \right) \right\}, \tag{30}
\end{aligned}$$

where the Doppler shifted frequency of the scattered field is

$$\omega_s = \Omega + \xi_i \cdot (\mathbf{v}_0 - \mathbf{v}_\sigma) + \xi \cdot \mathbf{v}_\sigma. \tag{31}$$

It is important to note that the time dependence has been factored from the surface integral in going from Eq. (29) to Eq. (30) following our approximation for the assumed low Mach number motion. This means, for example, that the object's orientation with respect to the incoming and outgoing waves is not significantly altered for a time period large enough compared to the source period for the source to be considered harmonic. This is discussed in more detail, for example, in Sec. II C and Appendix B.

We can then express the scattered field in the waveguide in terms of the plane-wave scattering function $S(\alpha, \beta; \alpha_i, \beta_i; \omega)$ of the object. With the aid of Eq. (C19), Eq. (30) becomes

$$\begin{aligned}
\Phi_s(\mathbf{r}, t) = & \frac{1}{\pi} \int_{-\infty}^{\infty} \int_{-\infty}^{\infty} d^2\xi d^2\xi_i \frac{1}{k(\omega_s)} \\
& \times e^{i[\xi \cdot \mathbf{r}^0 - \xi_i \cdot \mathbf{r}_0^0]} e^{-i[\Omega + \xi_i \cdot (\mathbf{v}_0 - \mathbf{v}_\sigma) + \xi \cdot (\mathbf{v}_\sigma - \mathbf{v})] t} \\
& \times F(z, z_0; \xi, \xi_i; \omega_s, \omega_i), \tag{32}
\end{aligned}$$

which is an expression for the field scattered by a moving target with arbitrary shape, where

$$\begin{aligned}
F(z, z_0; \xi, \xi_i; \omega_s, \omega_i) \\
= & \{A(z_0; \omega_i) C(z; \omega_s) S(\pi - \alpha(\omega_s), \beta; \alpha_i(\omega_i), \beta_i; \omega_s) \\
& + A(z_0; \omega_i) D(z; \omega_s) S(\alpha(\omega_s), \beta; \alpha_i(\omega_i), \beta_i; \omega_s) \\
& + B(z_0; \omega_i) C(z; \omega_s) S(\pi - \alpha(\omega_s), \beta; \pi - \alpha_i(\omega_i), \beta_i; \omega_s) \\
& + B(z_0; \omega_i) D(z; \omega_s) S(\alpha(\omega_s), \beta; \pi - \alpha_i(\omega_i), \beta_i; \omega_s)\}. \tag{33}
\end{aligned}$$

The formulation is fully bistatic and incorporates horizontal velocities of the source, target, and receiver. The source is assumed to be a simple-harmonic one radiating at frequency Ω , but the received time series will contain multiple frequency components due to Doppler effects. The Doppler frequency shifts are indicated in the argument of the complex exponential function of Eq. (32).

When the source, target, and receiver are at rest, all incident frequencies ω_i and scattered frequencies ω_s are equal to the source frequency Ω . In this case Eq. (32) reduces to Eq. (18) of Ref. 7 multiplied by $\exp(-i\Omega t)$ where reciprocity for harmonic waves

$$d_0 G(\mathbf{r}_\sigma | \mathbf{r}_0; \omega) = d_\sigma G(\mathbf{r}_0 | \mathbf{r}_\sigma; \omega) \tag{34}$$

was invoked for the incident field and the medium densities d_0 and d_σ in the layers of the source and target depth were assumed identical.

In Eq. (33), all coefficients (A 's and B 's) of the incident field are evaluated at the incident frequency ω_i , and all the coefficients of the scattered field (C 's and D 's) are evaluated at the scattered frequency ω_s . The wave number normalization k^{-1} and the plane-wave scatter function S are evaluated

at the scattered frequency ω_s as well. The equivalent elevation angles α_i of the incident plane waves are evaluated at the incident frequency ω_i , and the equivalent elevation angles α of the scattered plane waves are evaluated at the scattered frequency ω_s .

B. Spectral representation of the Doppler-shifted field scattered from a moving target by a source with arbitrary time dependence in a stratified waveguide

The Doppler-shifted scattered field induced by a source with arbitrary time dependence $q(t)$ and frequency spectrum $Q(\Omega)$ can be obtained in the receiver's frame of reference from Eq. (32) by Fourier synthesis as

$$\begin{aligned} \Psi_s(\mathbf{r}, t) = & \frac{1}{2\pi^2} \int_{-\infty}^{\infty} d\Omega Q(\Omega) \int_{-\infty}^{\infty} \int_{-\infty}^{\infty} d^2\xi d^2\xi_i \frac{1}{k(\omega_s)} \\ & \times e^{i[\xi \cdot \boldsymbol{\rho}^0 - \xi_i \cdot \boldsymbol{\rho}_i^0]} e^{-i[\Omega + \xi_i \cdot (\mathbf{v}_0 - \mathbf{v}_\sigma) + \xi \cdot (\mathbf{v}_\sigma - \mathbf{v})]t} \\ & \times F(z, z_0; \xi, \xi_i; \omega_s, \omega_i). \end{aligned} \quad (35)$$

A direct implementation of Eq. (35), however, will be inefficient because the four-dimensional wave number integrals are coupled with time in the argument of the complex exponential function and so need to be evaluated at each individual time instant. Similar difficulties for the passive problem of modeling propagation from a moving source to a moving receiver are discussed in Ref. 4 by Schmidt and Kuperman. They note that by transforming the Doppler-shifted field from the "source frequency" to a representation in terms of the "receiver frequency," the wave number and frequency integrations can be integrated independently.⁴

The frequency spectrum of the scattered field in the receiver's frame of reference is obtained by applying a Fourier transform to Eq. (35),

$$\Psi_s(\mathbf{r}, \omega') = \int_{-\infty}^{\infty} dt e^{i\omega' t} \Psi_s(\mathbf{r}, t) \quad (36)$$

where ω' is the frequency in the receiver's frame of reference. Integrating over t introduces the delta function $\delta(\omega' - \Omega - \xi_i \cdot (\mathbf{v}_0 - \mathbf{v}_\sigma) - \xi \cdot (\mathbf{v}_\sigma - \mathbf{v}))$ in the integrand. Upon integrating over Ω , the frequency spectrum of the Doppler-shifted scattered field in the receiver's frame of reference then becomes

$$\begin{aligned} \Psi_s(\mathbf{r}, \omega') = & \frac{1}{\pi} \int_{-\infty}^{\infty} \int_{-\infty}^{\infty} d^2\xi d^2\xi_i \frac{1}{k(\omega_s)} e^{i[\xi \cdot \boldsymbol{\rho}^0 - \xi_i \cdot \boldsymbol{\rho}_i^0]} \\ & \times Q(\omega' - \xi_i \cdot (\mathbf{v}_0 - \mathbf{v}_\sigma) - \xi \cdot (\mathbf{v}_\sigma - \mathbf{v})) \\ & \times F(z, z_0; \xi, \xi_i; \omega_s, \omega_i), \end{aligned} \quad (37)$$

where the shifted frequencies ω_i and ω_s in terms of ω' are equal to

$$\omega_i = \omega' + \xi_i \cdot (\mathbf{v} - \mathbf{v}_\sigma) + \xi_i \cdot \mathbf{v}_\sigma \quad (38)$$

and

$$\omega_s = \omega' + \xi \cdot \mathbf{v}. \quad (39)$$

Equation (37) can be implemented efficiently and directly without the need for time domain processing.

C. Normal mode representation of the Doppler-shifted field scattered from a moving target by a simple-harmonic source in a stratified waveguide

At sufficiently long source and receiver ranges from the target, the scattered field can be well represented as a sum of normal modes. The modal representation for the scattered field with a simple-harmonic source is derived in this section.

Green's function for the time-domain wave equation in a waveguide can be written as an inverse Fourier transform of the modal form of Green's function for the Helmholtz equation,

$$\begin{aligned} G(\mathbf{r}, t | \mathbf{r}_\sigma, t_\sigma) = & \frac{1}{2\pi} \int_{-\infty}^{\infty} d\omega G(\mathbf{r} | \mathbf{r}_\sigma; \omega) e^{-i\omega(t-t_\sigma)} \\ = & \frac{1}{2\pi} \int_{-\infty}^{\infty} d\omega e^{-i\omega(t-t_\sigma)} \\ & \times \frac{id}{4} \sum_m u_m(z; \omega) u_m(z_\sigma; \omega) \\ & \times H_0^{(1)}(\xi_m(\omega) |\boldsymbol{\rho} - \boldsymbol{\rho}_\sigma|), \end{aligned} \quad (40)$$

where $u_m(z; \omega)$ and $\xi_m(\omega)$ are the amplitude function and horizontal wave number of the m th mode at frequency ω . We assume $\xi_m(\omega) |\boldsymbol{\rho} - \boldsymbol{\rho}_\sigma| \gg 1$, and the asymptotic form of the zeroth-order Hankel function of the first kind is used

$$\begin{aligned} H_0^{(1)}(\xi_m(\omega) |\boldsymbol{\rho} - \boldsymbol{\rho}_\sigma|) \\ \approx \sqrt{\frac{2}{\pi \xi_m(\omega) |\boldsymbol{\rho} - \boldsymbol{\rho}_\sigma|}} e^{i(\xi_m(\omega) |\boldsymbol{\rho} - \boldsymbol{\rho}_\sigma| - \pi/4)}. \end{aligned} \quad (41)$$

For a moving target, the horizontal position vector $\boldsymbol{\rho}_\sigma$ is

$$\begin{aligned} \boldsymbol{\rho}_\sigma = & \boldsymbol{\rho}_\sigma^0 + \mathbf{v}_\sigma t_\sigma \\ = & (\rho_\sigma^0 \cos \phi_\sigma^0 \mathbf{i}_x + \rho_\sigma^0 \sin \phi_\sigma^0 \mathbf{i}_y) \\ & + (v_\sigma t_\sigma \cos \varphi_\sigma \mathbf{i}_x + v_\sigma t_\sigma \sin \varphi_\sigma \mathbf{i}_y), \end{aligned} \quad (42)$$

where $\boldsymbol{\rho}_\sigma^0$ is its initial position at $t_\sigma=0$ and \mathbf{v}_σ is its horizontal velocity. Similarly, the horizontal position vector of the receiver $\boldsymbol{\rho}$ is

$$\begin{aligned} \boldsymbol{\rho} = & \boldsymbol{\rho}^0 + \mathbf{v}t \\ = & (\rho^0 \cos \phi^0 \mathbf{i}_x + \rho^0 \sin \phi^0 \mathbf{i}_y) + (vt \cos \varphi \mathbf{i}_x + vt \sin \varphi \mathbf{i}_y), \end{aligned} \quad (43)$$

where $\boldsymbol{\rho}^0$ is its initial position at $t_\sigma=0$ and \mathbf{v} is its horizontal velocity.

For the bistatic configuration used in the scattering problem, the horizontal range to a point on the target is much smaller than the range to the receiver so that $|\boldsymbol{\rho}_\sigma| \ll |\boldsymbol{\rho}|$. For low Mach number motions of the target as in typical sonar scenarios, the displacements $|\mathbf{v}_\sigma t_\sigma|$ of a target point and $|\mathbf{v}t|$ of the receiver are also much smaller than $|\boldsymbol{\rho}|$ so that the azimuthal angle of the vector $\boldsymbol{\rho}^0 + \mathbf{v}t - \boldsymbol{\rho}_\sigma^0$ is approximately equal to the azimuthal angle ϕ^0 of the vector $\boldsymbol{\rho}^0$ even for a time duration t so much larger than the source period that the source can be considered harmonic. An approximation for $|\boldsymbol{\rho} - \boldsymbol{\rho}_\sigma|$ can then be made that

$$|\boldsymbol{\rho} - \boldsymbol{\rho}_\sigma| = |\boldsymbol{\rho}^0 + \mathbf{v}t - \boldsymbol{\rho}_\sigma^0 - \mathbf{v}_\sigma t_\sigma|$$

$$\approx |\boldsymbol{\rho}^0 + \mathbf{v}t - \boldsymbol{\rho}_\sigma^0| - v_\sigma t_\sigma \cos(\phi^0 - \varphi_\sigma). \quad (44a)$$

Similarly, the azimuthal angle of the vector $\boldsymbol{\rho}^0 - \boldsymbol{\rho}_\sigma^0$ is approximated as ϕ^0 because $|\boldsymbol{\rho}_\sigma^0| \ll |\boldsymbol{\rho}^0|$. This leads to

$$|\boldsymbol{\rho} - \boldsymbol{\rho}_\sigma| \approx |\boldsymbol{\rho}^0 - \boldsymbol{\rho}_\sigma^0| + vt \cos(\phi^0 - \varphi) - v_\sigma t_\sigma \cos(\phi^0 - \varphi_\sigma). \quad (44b)$$

Then since $|\boldsymbol{\rho}_\sigma^0| \ll |\boldsymbol{\rho}^0|$ we have

$$|\boldsymbol{\rho} - \boldsymbol{\rho}_\sigma| \approx \rho^0 - \rho_\sigma^0 \cos(\phi^0 - \phi_\sigma^0) + vt \cos(\phi^0 - \varphi) - v_\sigma t_\sigma \cos(\phi^0 - \varphi_\sigma). \quad (44c)$$

Green's function for the time-domain scalar wave equation from a point on the surface of the target \mathbf{r}_σ at retarded time t_σ to the receiver location \mathbf{r} at time t then can be approximated as

$$G(\mathbf{r}, t | \mathbf{r}_\sigma, t_\sigma) = \frac{1}{2\pi} \int_{-\infty}^{\infty} d\omega e^{-i\omega(t-t_\sigma)}$$

$$\times \frac{id}{\sqrt{8\pi}} e^{-i(\pi/4)} \sum_m \frac{u_m(z; \omega) u_m(z_\sigma; \omega)}{\sqrt{\xi_m(\omega)} \rho^0}$$

$$\times e^{i\xi_m(\omega)[\rho^0 - \rho_\sigma^0 \cos(\phi^0 - \phi_\sigma^0)]}$$

$$\times e^{i\xi_m(\omega)v \cos(\phi^0 - \varphi)t} e^{-i\xi_m(\omega)v_\sigma \cos(\phi^0 - \varphi_\sigma)t_\sigma}. \quad (45)$$

As in Eqs. (41) and (42) of Ref. 6, the Green function

and the incident field are now expressed as a linear superposition of equivalent plane waves in the layer of the target via

$$G(\mathbf{r}, t | \mathbf{r}_\sigma, t_\sigma) = \frac{1}{2\pi} \int_{-\infty}^{\infty} d\omega e^{-i\omega(t-t_\sigma)}$$

$$\times \sum_m [A_m(\mathbf{r}^0; \omega) e^{-ik(\omega)r_\sigma^0 \eta(\pi - \alpha_m, \phi^0; \theta_\sigma^0, \phi_\sigma^0)}$$

$$- B_m(\mathbf{r}^0; \omega) e^{-ik(\omega)r_\sigma^0 \eta(\alpha_m, \phi^0; \theta_\sigma^0, \phi_\sigma^0)}]$$

$$\times e^{i\xi_m(\omega)v \cos(\phi^0 - \varphi)t} e^{-i\xi_m(\omega)v_\sigma \cos(\phi^0 - \varphi_\sigma)t_\sigma} \quad (46)$$

and

$$\Phi_l(\mathbf{r}_\sigma, t_\sigma) = \sum_l \frac{1}{1 + \frac{v_0}{v_l^G(\Omega)} \cos(\phi_0^0 - \varphi_0)}$$

$$\times [A_l(\mathbf{r}_0^0; \omega_l) e^{ik(\omega_l)r_\sigma^0 \eta(\alpha_l, \pi - \phi_0^0; \theta_\sigma^0, \phi_\sigma^0)}$$

$$- B_l(\mathbf{r}_0^0; \omega_l) e^{ik(\omega_l)r_\sigma^0 \eta(\pi - \alpha_l, \pi - \phi_0^0; \theta_\sigma^0, \phi_\sigma^0)}]$$

$$\times e^{-i(\omega_l + \xi_l(\omega_l)v_\sigma \cos(\phi_0^0 - \varphi_0))t_\sigma}, \quad (47)$$

where Eq. (47) is derived in from Eq. (B11), and ω_l is the Doppler-shifted frequency of the l th mode as defined in Eq. (B10). Substituting Eqs. (46) and (47) into Eq. (12) leads to

$$\Phi_s(\mathbf{r}, t) = -\frac{1}{2\pi} \int_0^{t^+} dt_\sigma \oint d\mathbf{S}_\sigma \cdot \left\{ \left[\sum_l \frac{1}{1 + [v_0/v_l^G(\Omega)] \cos(\phi_0^0 - \varphi_0)} [A_l(\mathbf{r}_0^0; \omega_l) e^{ik(\omega_l)r_\sigma^0 \eta(\alpha_l, \pi - \phi_0^0; \theta_\sigma^0, \phi_\sigma^0)} \right. \right.$$

$$\left. \left. - B_l(\mathbf{r}_0^0; \omega_l) e^{ik(\omega_l)r_\sigma^0 \eta(\pi - \alpha_l, \pi - \phi_0^0; \theta_\sigma^0, \phi_\sigma^0)} \right] e^{-i(\omega_l + \xi_l(\omega_l)v_\sigma \cos(\phi_0^0 - \varphi_0))t_\sigma} + \Phi_s(\mathbf{r}_\sigma, t_\sigma) \right]$$

$$\times \nabla_\sigma \left(\int_{-\infty}^{\infty} d\omega e^{-i\omega(t-t_\sigma)} \sum_m [A_m(\mathbf{r}^0; \omega) e^{-ik(\omega)r_\sigma^0 \eta(\pi - \alpha_m, \phi^0; \theta_\sigma^0, \phi_\sigma^0)} \right.$$

$$\left. \left. - B_m(\mathbf{r}^0; \omega) e^{-ik(\omega)r_\sigma^0 \eta(\alpha_m, \phi^0; \theta_\sigma^0, \phi_\sigma^0)} \right] e^{i\xi_m(\omega)v \cos(\phi^0 - \varphi)t} e^{-i\xi_m(\omega)v_\sigma \cos(\phi^0 - \varphi_\sigma)t_\sigma} \right) \left. \right\}. \quad (48)$$

For low Mach number motion, the scattered field on the surface of the object in Eq. (48) is approximately $\hat{\Phi}_s(\mathbf{r}_\sigma, t_\sigma) \approx \hat{\Phi}_s(\mathbf{r}_\sigma; \omega_l) e^{-i\omega_l t_\sigma}$ for a given incident plane wave. We define the wave number vectors for the downgoing and upgoing waves for the l th mode as

$$\mathbf{k}_l^+ = \xi_l \hat{\mathbf{i}}_\rho + \gamma_l \hat{\mathbf{i}}_z, \quad (49)$$

$$\mathbf{k}_l^- = \xi_l \hat{\mathbf{i}}_\rho - \gamma_l \hat{\mathbf{i}}_z. \quad (50)$$

The scattered field on the surface of the target given in Eq. (48) can then be represented in terms of downgoing and upgoing plane incident waves with unit amplitudes $\hat{\Phi}_s(\mathbf{r}_\sigma, \mathbf{k}_l^+; \omega_l)$ and $\hat{\Phi}_s(\mathbf{r}_\sigma, \mathbf{k}_l^-; \omega_l)$, respectively, via

$$\Phi_s(\mathbf{r}_\sigma, t_\sigma) = \sum_l \frac{e^{-i\omega_l t_\sigma}}{1 + \frac{v_0}{v_l^G(\Omega)} \cos(\phi_0^0 - \varphi_0)} [A_l(\mathbf{r}_0^0; \omega_l) \hat{\Phi}_s(\mathbf{r}_\sigma, \mathbf{k}_l^+; \omega_l) - B_l(\mathbf{r}_0^0; \omega_l) \hat{\Phi}_s(\mathbf{r}_\sigma, \mathbf{k}_l^-; \omega_l)]. \quad (51)$$

Just as in the derivation for the spectral representation, in Sec. II A, approximations are made for $\hat{\Phi}_s(\mathbf{r}_\sigma, \mathbf{k}_l^+; \omega_l)$ and $\hat{\Phi}_s(\mathbf{r}_\sigma, \mathbf{k}_l^-; \omega_l)$ that account for rigid body translation. Equation (51) then becomes

$$\begin{aligned} \Phi_s(\mathbf{r}_\sigma, t_\sigma) = \sum_l \frac{1}{1 + \frac{v_0}{v_l^G(\Omega)} \cos(\phi_0^0 - \varphi_0)} e^{-i(\omega_l + \xi_l(\omega_l)v_\sigma \cos(\phi_0^0 - \varphi_\sigma))t_\sigma} \\ \times [A_l(\mathbf{r}_0^0; \omega_l) \hat{\Phi}_s(\mathbf{r}_\sigma^0, \mathbf{k}_l^+; \omega_l) - B_l(\mathbf{r}_0^0; \omega_l) \hat{\Phi}_s(\mathbf{r}_\sigma^0, \mathbf{k}_l^-; \omega_l)]. \end{aligned} \quad (52)$$

When this is inserted into Eq. (48) the scattered field takes the form

$$\begin{aligned} \Phi_s(\mathbf{r}, t) = -\frac{1}{2\pi} \int_0^{t^+} dt_\sigma \oint d\mathbf{S}_\sigma \cdot \left\{ \sum_l \frac{1}{1 + [v_0/v_l^G(\Omega)] \cos(\phi_0^0 - \varphi_0)} e^{-i(\omega_l + \xi_l(\omega_l)v_\sigma \cos(\phi_0^0 - \varphi_\sigma))t_\sigma} \right. \\ \times \left(A_l(\mathbf{r}_0^0; \omega_l) [e^{ik(\omega_l)r_\sigma^0 \eta(\alpha_l, \pi - \phi_0^0; \theta_\sigma^0, \phi_\sigma^0)} + \hat{\Phi}_s(\mathbf{r}_\sigma^0, \mathbf{k}_l^+; \omega_l)] \right. \\ \left. - B_l(\mathbf{r}_0^0; \omega_l) [e^{ik(\omega_l)r_\sigma^0 \eta(\pi - \alpha_l, \pi - \phi_0^0; \theta_\sigma^0, \phi_\sigma^0)} + \hat{\Phi}_s(\mathbf{r}_\sigma^0, \mathbf{k}_l^-; \omega_l)] \right) \\ \times \nabla_\sigma \left(\int_{-\infty}^{\infty} d\omega e^{-i\omega(t-t_\sigma)} \sum_m [A_m(\mathbf{r}^0; \omega) e^{-ik(\omega)r_\sigma^0 \eta(\pi - \alpha_m, \phi^0; \theta_\sigma^0, \phi_\sigma^0)} - B_m(\mathbf{r}^0; \omega) e^{-ik(\omega)r_\sigma^0 \eta(\alpha_m, \phi^0; \theta_\sigma^0, \phi_\sigma^0)}] \right. \\ \left. \times e^{i\xi_m(\omega)v_\sigma \cos(\phi^0 - \varphi)} e^{-i\xi_m(\omega)v_\sigma \cos(\phi^0 - \varphi_\sigma)t_\sigma} \right\}. \end{aligned} \quad (53)$$

For sufficiently long time duration t , integration over t_σ introduces the delta function $\delta(\omega - \omega_l - \xi_l(\omega_l)v_\sigma \cos(\phi_0^0 - \varphi_\sigma) - \xi_m(\omega)v_\sigma \cos(\phi^0 - \varphi_\sigma))$ to the integrand.

In order to integrate over ω , we need to solve the transcendental equation for the argument $h(\omega)$ of the δ function

$$\begin{aligned} h(\omega) = \omega - \omega_l - \xi_l(\omega_l)v_\sigma \cos(\phi_0^0 - \varphi_\sigma) \\ - \xi_m(\omega)v_\sigma \cos(\phi^0 - \varphi_\sigma) = 0. \end{aligned} \quad (54)$$

Equation (54) can be solved numerically. However, an approximation that can be evaluated analytically is desired. The derivative of $h(\omega)$ with respect to ω is

$$\begin{aligned} \frac{dh(\omega)}{d\omega} &= 1 - \frac{d\xi_m(\omega)}{d\omega} v_\sigma \cos(\phi^0 - \varphi_\sigma) \\ &= 1 - \frac{v_\sigma}{v_m^G(\omega)} \cos(\phi^0 - \varphi_\sigma), \end{aligned} \quad (55)$$

where $v_m^G(\omega)$ is the group velocity of the m th mode at frequency ω . For low Mach number motions, Eq. (55) is close to unity, so that $h(\omega)$ is nearly linear around the roots of Eq. (54). Using the Newton–Raphson method with the frequency ω_l as an initial guess, the first iteration yields a reasonably accurate solution of Eq. (54) as

$$\omega_{m,l} = \omega_l - \frac{h(\omega_l)}{h'(\omega_l)} = \omega_l + \frac{\xi_l(\omega_l)v_\sigma \cos(\phi_0^0 - \varphi_\sigma) + \xi_m(\omega_l)v_\sigma \cos(\phi^0 - \varphi_\sigma)}{1 - \frac{v_\sigma}{v_m^G(\omega_l)} \cos(\phi^0 - \varphi_\sigma)}, \quad (56)$$

where $v_m^G(\omega_l)$ is the group velocity of the m th mode at frequency ω_l . Here $\omega_{m,l}$ is the doubly Doppler-shifted frequency with respect to the l th incident mode and the m th outgoing mode. Using the property of the δ function for any functions f, h [Eq. (9.6) in Ref. 2] it must hold that

$$\int_{-\infty}^{\infty} f(\omega) \delta(h(\omega)) d\omega = \left[\frac{f(\omega)}{|dh/d\omega|} \right]_{\omega=\omega^*}, \quad (57)$$

where ω^* is a zero of h , i.e., $h(\omega^*)=0$. Integrating over ω gives

$$\begin{aligned} \Phi_s(\mathbf{r}, t) = & - \sum_l \sum_m \oint d\mathbf{S}_\sigma \cdot \left\{ \frac{1}{1 + [v_0/v_l^G(\Omega)] \cos(\phi_0^0 - \varphi_0)} \frac{1}{1 - [v_\sigma/v_m^G(\omega_{m,l})] \cos(\phi^0 - \varphi_\sigma)} \right. \\ & \times (A_l(\mathbf{r}_0^0; \omega_l) [e^{ik(\omega_l)r_\sigma^0 \eta(\alpha_l, \pi - \phi_0^0; \theta_\sigma^0, \phi_\sigma^0)} + \hat{\Phi}_s(\mathbf{r}_\sigma^0, \mathbf{k}_l^+; \omega_l)] \\ & - B_l(\mathbf{r}_0^0; \omega_l) [e^{ik(\omega_l)r_\sigma^0 \eta(\pi - \alpha_l, \pi - \phi_0^0; \theta_\sigma^0, \phi_\sigma^0)} + \hat{\Phi}_s(\mathbf{r}_\sigma^0, \mathbf{k}_l^-; \omega_l)]) \\ & \times \nabla_\sigma \left([A_m(\mathbf{r}^0; \omega_{m,l}) e^{-ik(\omega_{m,l})r_\sigma^0 \eta(\pi - \alpha_m, \phi^0; \theta_\sigma^0, \phi_\sigma^0)} - B_m(\mathbf{r}^0; \omega) e^{-ik(\omega_{m,l})r_\sigma^0 \eta(\alpha_m, \phi^0; \theta_\sigma^0, \phi_\sigma^0)}] \right. \\ & \left. \left. \times e^{-i(\omega_{m,l} - \xi_m(\omega_{m,l})v \cos(\phi^0 - \varphi))t} \right) \right\}. \quad (58) \end{aligned}$$

With the aid of Eq. (C19), the scattered field can finally be written in terms of the scattering function of the target as

$$\begin{aligned} \Phi_s(\mathbf{r}, t) = & 4\pi \sum_l \sum_m \frac{1}{1 + \frac{v_0}{v_l^G(\Omega)} \cos(\phi_0^0 - \varphi_0)} \frac{1}{1 - \frac{v_\sigma}{v_m^G(\omega_{m,l})} \cos(\phi^0 - \varphi_\sigma)} \frac{1}{k(\omega_{m,l})} \\ & \times [A_l(\mathbf{r}_0^0; \omega_l) A_m(\mathbf{r}^0; \omega_{m,l}) S(\pi - \alpha_m(\omega_{m,l}), \phi^0; \alpha_l(\omega_l), \pi - \phi_0^0; \omega_{m,l}) \\ & - A_l(\mathbf{r}_0^0; \omega_l) B_m(\mathbf{r}^0; \omega_{m,l}) S(\alpha_m(\omega_{m,l}), \phi^0; \alpha_l(\omega_l), \pi - \phi_0^0; \omega_{m,l}) \\ & - B_l(\mathbf{r}_0^0; \omega_l) A_m(\mathbf{r}^0; \omega_{m,l}) S(\pi - \alpha_m(\omega_{m,l}), \phi^0; \pi - \alpha_l(\omega_l), \pi - \phi_0^0; \omega_{m,l}) \\ & + B_l(\mathbf{r}_0^0; \omega_l) B_m(\mathbf{r}^0; \omega_{m,l}) S(\alpha_m(\omega_{m,l}), \phi^0; \pi - \alpha_l(\omega_l), \pi - \phi_0^0; \omega_{m,l})] e^{-i(\omega_{m,l} - \xi_m(\omega_{m,l})v \cos(\phi^0 - \varphi))t}. \quad (59) \end{aligned}$$

When there is no motion of the source, target, or receiver, all the incident and scattered frequencies are evaluated at the source frequency Ω , and Eq. (59) leads to the special case Eq. (51) of Ref. 6 multiplied by $\exp(-i\Omega t)$.

If the number of modes that truncates the modal summation excited at the source frequency Ω is N , this same number can be used to truncate the incident and outgoing modal summations for low Mach number motions. The total number of discrete frequency components will then be roughly N^2 due to the coupling between incident and scattered modes at the target.

D. Normal mode representation of the Doppler-shifted field scattered from a moving target by a source with arbitrary time dependence in a stratified waveguide

For a source with arbitrary time dependence $q(t)$ and frequency spectrum $Q(\Omega)$, the normal mode representation of the Doppler-shifted scattered field can be formulated by Fourier synthesis as

$$\Psi_s(\mathbf{r}, t) = \frac{1}{2\pi} \int_{-\infty}^{\infty} d\Omega Q(\Omega) \Phi_s(\mathbf{r}, t), \quad (60)$$

where $\Phi_s(\mathbf{r}, t)$ is given in Eq. (59).

Equation (60), however, is computationally inefficient because the modal summation needs to be evaluated at every time instant. Just as in the spectral representation of the scattered field from a source with arbitrary time dependence, transformation to the frequency spectrum in the receiver's frame of reference can speed up the computation significantly.

Applying a Fourier transform to Eq. (60) is not desired because both shifted frequencies ω_l and $\omega_{m,l}$ of the incident and scattered field are approximations obtained by the Newton–Raphson method in terms of the source frequency Ω . A derivation for the shifted frequencies in terms of the receiving frequency ω' based on those approximated values will give inaccurate and complicated results. Therefore, the frequency spectrum in the receiver's frame of reference needs to be derived from intermediate expressions for the incident field and scattered field before the approximations by the Newton–Raphson method are made. The derivation is lengthy and is given in Appendix D. With the aid of Eq. (C19), the scattered field of Eq. (D14) is expressed in terms of the scattering function of the target as

$$\Psi_s(\mathbf{r}, \omega') = 4\pi \sum_l \sum_m \frac{Q(\Omega_{lm})}{k(\omega'_m)} \frac{1}{1 - \frac{v}{v_m^G(\omega'_m)} \cos(\phi^0 - \varphi)} \frac{1}{1 + \frac{v_\sigma}{v_l^G(\omega'_{l,m})} \cos(\phi_0^0 - \varphi_\sigma)}$$

$$\times [A_l(\mathbf{r}_0^0; \omega'_{l,m}) A_m(\mathbf{r}^0; \omega'_m) S(\pi - \alpha_m(\omega'_m), \phi^0; \alpha_l(\omega'_{l,m}), \pi - \phi_0^0; \omega'_m)$$

$$- A_l(\mathbf{r}_0^0; \omega'_{l,m}) B_m(\mathbf{r}^0; \omega'_m) S(\alpha_m(\omega'_m), \phi^0; \alpha_l(\omega'_{l,m}), \pi - \phi_0^0; \omega'_m)$$

$$- B_l(\mathbf{r}_0^0; \omega'_{l,m}) A_m(\mathbf{r}^0; \omega'_m) S(\pi - \alpha_m(\omega'_m), \phi^0; \pi - \alpha_l(\omega'_{l,m}), \pi - \phi_0^0; \omega'_m)$$

$$+ B_l(\mathbf{r}_0^0; \omega'_{l,m}) B_m(\mathbf{r}^0; \omega'_m) S(\alpha_m(\omega'_m), \phi^0; \pi - \alpha_l(\omega'_{l,m}), \pi - \phi_0^0; \omega'_m)], \quad (61)$$

where the frequency of the source spectrum is

$$\Omega_{lm} = \omega'_{l,m} + \xi_l(\omega'_{l,m}) v_0 \cos(\phi_0^0 - \varphi_0). \quad (62)$$

Equation (61) can be implemented efficiently and directly without the need for time domain processing.

III. ILLUSTRATIVE EXAMPLES

Equation (61) is implemented with a modified version of the normal mode code KRAKENC.¹³ The formulation is fully bistatic and incorporates the motion of source, target, and receiver. For simplicity, only monostatic configurations are illustrated. These have the strongest Doppler frequency shifts when only the target is in motion and the source and receiver are at rest.

The source function to be used in all examples is a Gaussian modulated wave form

$$q(t) = \frac{1}{\sqrt{2\pi\sigma}} e^{-(t-t_0)^2/2\sigma^2} e^{-i2\pi f_c(t-t_0)} \quad (63)$$

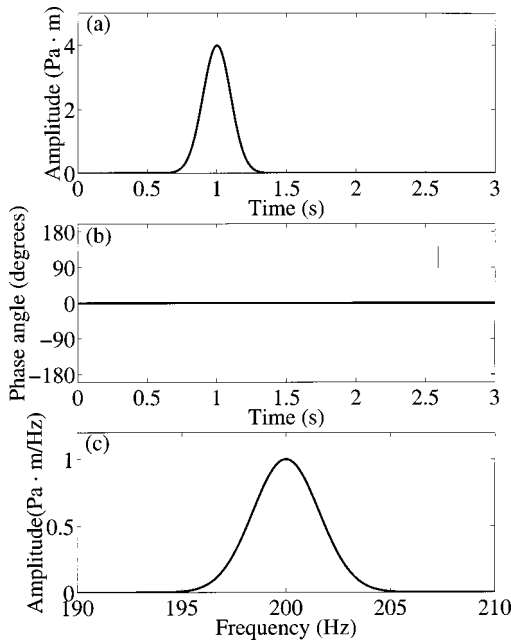


FIG. 2. Plot (a) and (b) show the amplitude and phase of the source function, demodulated by the 200 Hz carrier frequency, versus time. Plot (c) shows the magnitude of the frequency spectrum of the source.

with carrier frequency $f_c = 200$ Hz, $t_0 = 1$ s and $\sigma = 0.1$ s. Its frequency spectrum is

$$Q(f) = e^{-(1/2)\sigma^2[2\pi(f-f_c)]^2} e^{i2\pi f t_0}. \quad (64)$$

The amplitude and phase of the time series of the source demodulated by the carrier frequency $f_c = 200$ Hz is shown in Figs. 2(a) and 2(b). The frequency spectrum of the source is shown in Fig. 2(c).

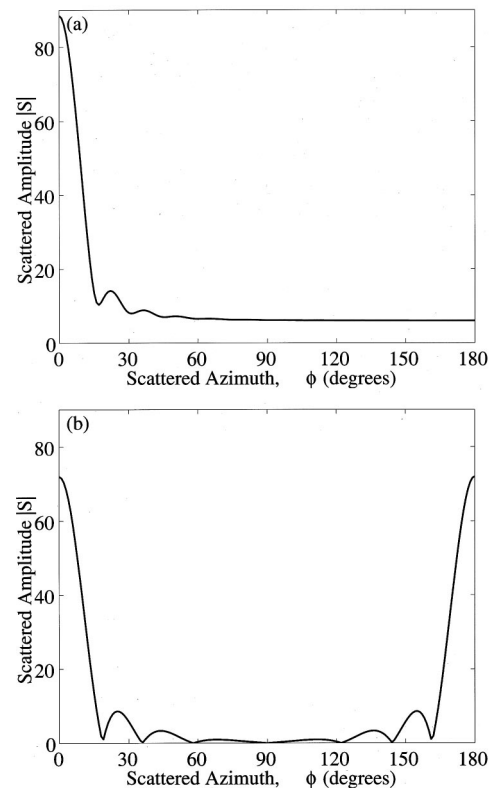


FIG. 3. The magnitude of the free space plane-wave scattering function $S(\theta=90^\circ, \beta=\phi; \alpha_i=90^\circ, \beta_i=0^\circ)$ for (a) a pressure-release sphere with $ka=12$ at 200 Hz and (b) a pressure-release circular disk with $ka=12$ at 200 Hz. The incident wave is parallel to the disk's surface normal, i.e., at broadside to the disk.

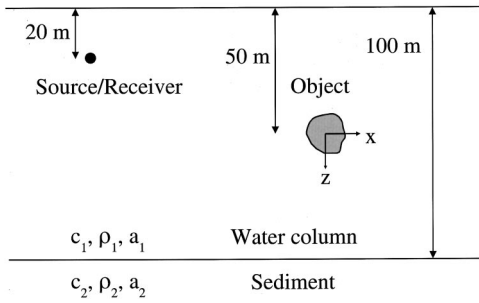


FIG. 4. Measurement geometry for object scattering in a Pekeris waveguide. The source and receiver are collocated at a depth of 20 m, and the centroid of the target is at a depth of 50 m.

All time series illustrations in this paper follow the same convention used in Figs. 2(a) and 2(b). They show the magnitude and phase of the signals demodulated by the carrier frequency at 200 Hz. The phase is only shown at times when the signal amplitude is not negligibly small. All horizontal axes of time series plots in this section are labeled with “reduced time,” which is the actual time minus the round-trip horizontal range divided by the sound speed.

Two types of targets are used as to illustrate scattering characteristics, including a pressure-release sphere and a perfectly reflecting circular disk which both have $ka = 12$ at 200

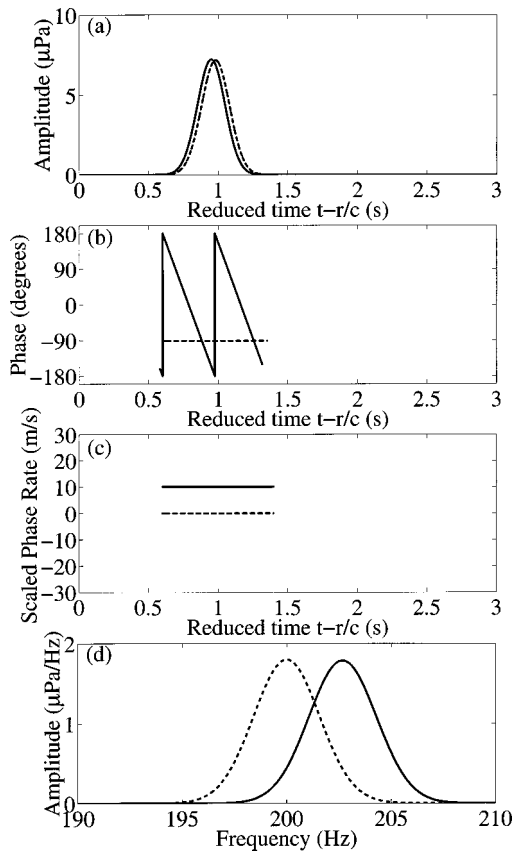


FIG. 5. The scattered field and its scaled phase rate for the Gaussian modulated source in free space. The object is a pressure-release sphere of $ka = 12$ at 200 Hz. The dashed curves are for a stationary target. The solid curves are for a target moving toward the source at 10 m/s. Plots (a) and (b) show the amplitude and phase of the time series demodulated by the 200 Hz carrier frequency. Plot (c) shows the scaled phase rate of the demodulated time series from Eq. (65). Plot (d) shows the frequency spectra.

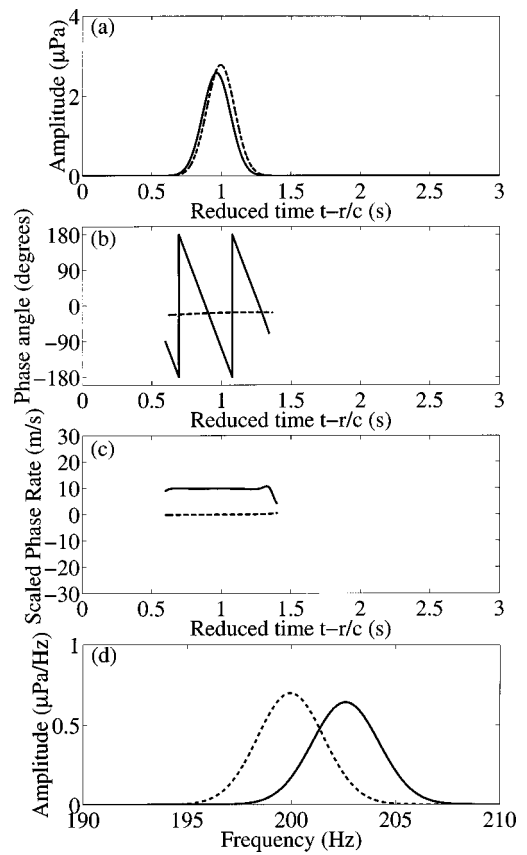


FIG. 6. The scattered field and its scaled phase rate for the Gaussian modulated source. The bottom type is silt. Source and receiver are collocated at 20-m depth with 50-m target depth. The horizontal range of the target is 2000 m from the source. The object is a pressure-release sphere of $ka = 12$ at 200 Hz. The dashed curves are for a stationary target. The solid curves are for a target moving toward the source at 10 m/s. Plots (a) and (b) show the amplitude and phase of the time series demodulated by the 200 Hz carrier frequency. Plot (c) shows the scaled phase rate of the demodulated time series Eq. (65). Plot (d) shows the frequency spectra.

Hz, where a is the radius of the sphere and disk. The free space plane wave scattering function of the sphere is given in Eq. (A2) of Ref. 7. The scatter function of the disk is given in Ref. 14. Figures 3(a) and (b) show the magnitude of the scatter functions versus scattering angle for the sphere and the disk, respectively. The incident wave is parallel to the disk’s surface normal, i.e., at broadside to the disk.

Before illustrating the problem in a waveguide, examples of object scattering in free space are shown for comparison. The measurement geometry is the same as that shown in Fig. 4 but without the waveguide boundaries.

A monostatic sonar with collocated point source and receiver senses a pressure-release sphere with $ka = 12$ at $f_c = 200$ Hz. The sonar and target are in water with a sound speed of 1500 m/s, and they are initially separated by 2000 m in the horizontal and 30 m in the vertical. Equation (C18) is used to perform the simulations. The dashed curves in Figs. 5(a) and 5(b) show the amplitude and phase of the demodulated time series of the scattered signals from a stationary target. The dashed curve in Fig. 5(d) shows its frequency spectrum. Since free space is nondispersive, and the scatter function is nearly constant over the frequency band of the source, the received wave form appears effectively as a

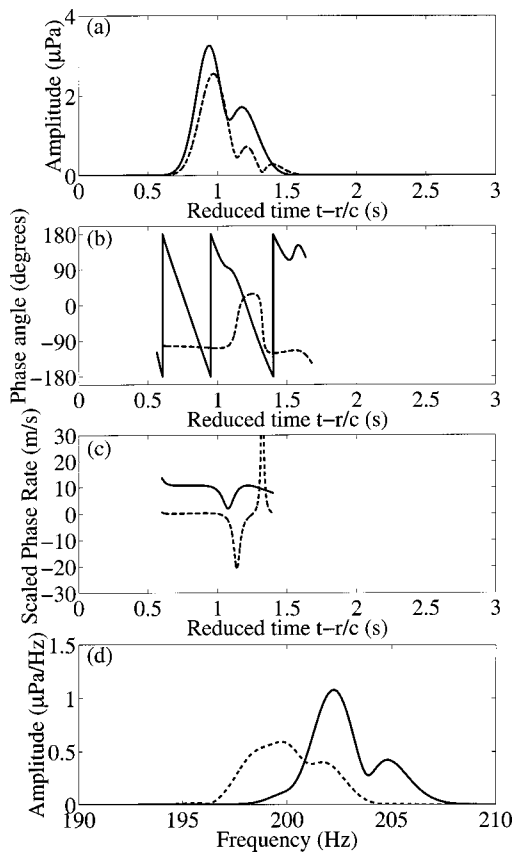


FIG. 7. Same as Fig. 6 except bottom type is sand.

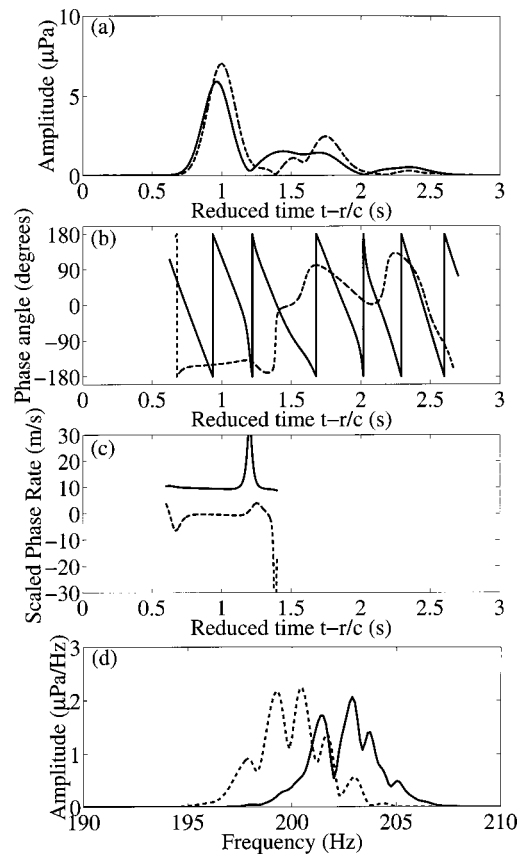


FIG. 8. Same as Fig. 6 except bottom type is limestone.

scaled and time-shifted version of the transmitted signal, with negligible spectral distortion. The time series after demodulation and the spectrum of the field scattered from a sphere moving at 10 m/s toward the source are shown as the solid curves in Figs. 5(a), 5(b) and 5(d). It can be seen that the free space Doppler-shifted spectrum can be very closely approximated by a translated version of the stationary spectrum since negligible distortion is introduced by the Doppler shift, dynamical factors described in Appendix C, and scatter function over the frequency band of the source. The phase angle versus time in Fig. 5(b) shows that the phase is nearly a constant versus time for a stationary object. For the moving target, the phase angle is decreasing with respect to time at a constant rate, which represents a single frequency shift induced by the target motion.

The frequency shift is linearly proportional to the radial component of target velocity in free space when the scattering function of the target does not vary significantly versus frequency within the band of the source. Active sonar and radar systems in free space typically take the scaled phase rate

$$\mu(t) = -\frac{c}{4\pi f_c} \frac{d\Theta(t)}{dt} \quad (65)$$

as an estimate of the target's radial velocity where $\Theta(t)$ is the phase angle of the sonar return after demodulation by the carrier frequency. The dashed curve and the solid curve in Fig. 5(c) show that the scaled phase rate $\mu(t)$ matches the

true value of the radial velocity of the targets, 0 m/s and 10 m/s for the examples shown.

In all illustrative examples of this section, a water column of 100 m depth is used to simulate a typical continental shelf environment. The density of the water is 1000 kg/m³, the sound speed is 1500 m/s, and the attenuation is 6.0×10^{-5} dB/λ. The simulations are performed over different seabed types to illustrate the dependence of the Doppler effects on bottom properties. All seabeds are modeled as half-spaces. The source and the receiver are collocated at a depth of 20 m without motion, and the centroid of the target is at a depth of 50 m.

First, we show how different bottom types affect the Doppler shifts. Sand, silt, and limestone are used as the homogeneous material of the bottom half-space. The density, sound speed, and attenuation are taken to be 1900 kg/m³, 1700 m/s, and 0.8 dB/λ for sand, 1400 kg/m³, 1520 m/s, and 0.3 dB/λ for silt. The density, compressional speed and shear speed of limestone are 2200 kg/m³, 2500 m/s, and 800 m/s, respectively. The attenuation coefficients are 0.1 and 0.2 dB/λ for compression and shear, respectively.

A silt bottom is used for the simulations in Fig. 6. A pressure-release sphere with $ka = 12$ at 200 Hz is used as the target. The dashed curves in Figs. 6(a) and 6(b) show the amplitude and phase of the demodulated time series of the scattered signals from a stationary target, and the dashed curve in Fig. 6(d) shows its frequency spectrum. Both the amplitude of the time series and frequency spectrum appear to be Gaussian, which indicates that the dispersion due to multipath effects in the waveguide is weak for this type of

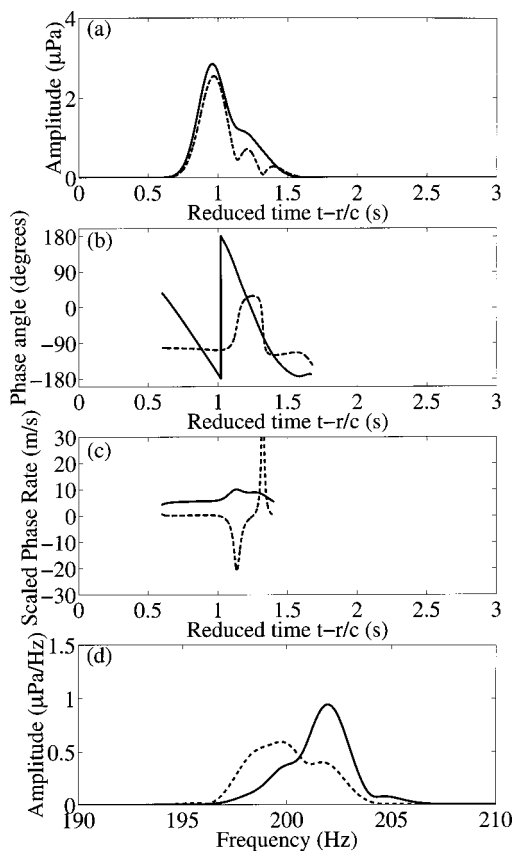


FIG. 9. Same as Fig. 6 except the bottom type is sand and target velocity is changed. The target is moving toward the source at 5 m/s.

bottom. The scattered field is dominated by the lowest order mode. The solid curves in Figs. 6(a) and 6(b) show the received time series scattered by a sphere moving toward the source at 10 m/s, and the solid curve in Fig. 6(d) shows its frequency spectrum. The shape of the time series still looks Gaussian, and the arrival time is slightly earlier than the stationary case due to the shortening of the horizontal distance. The frequency shifts due to Doppler effects can be observed in the solid curve in Fig. 6(d). The spectrum also looks Gaussian but is shifted with the frequency shift of the first mode, which is close to the frequency shift of the scattered field in free space. Similar to the examples for free space, the phase versus time shown in Fig. 6(b) is nearly a constant for the stationary target, and the phase is changing at nearly a constant rate for the moving target. Applying Eq. (65), the scaled phase rate $\mu(t)$ is calculated for both the stationary and the moving targets and is plotted as the dashed and the solid curves in Fig. 6(c), respectively. Because the sonar return is not significantly distorted by the multimodal dispersion and Doppler effects, the scaled phase rate is close to the target's true radial velocity for both the stationary and the moving target. This indicates that the scaled phase rate $\mu(t)$ in Eq. (65) can be used to estimate the radial velocity of targets for this particular scenario of a weakly dispersive waveguide.

Figure 7 shows demodulated time series and frequency spectra for a sand bottom. The same spherical scatterer is used as in Fig. 6. The dashed curves in Fig. 7(a) and 7(b) show the amplitude and phase of the demodulated time series

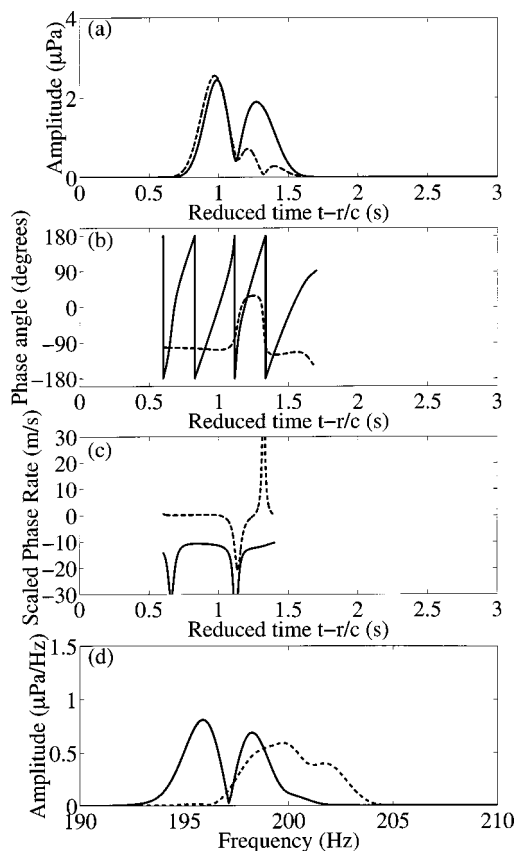


FIG. 10. Same as Fig. 6 except the bottom type is sand and target moves away from source at 10 m/s.

when the sphere is stationary. We see that the time series has not only the arrival from the first mode but also the late arrivals from the higher order modes with slower group velocities. This indicates that the dispersion is much stronger for a sand bottom than a silt bottom. The received signals from a moving sphere [solid curves in Fig. 7(a)] show that not only the first arrival is earlier than in the stationary case but the contributions of the higher order modes are also different. From Fig. 7(d), we can see that the spectrum of the stationary case (dashed curve) is distorted due to multimodal effects. The shifted spectrum (solid curve) is also distorted and is not simply a translated version of the stationary spectrum (dashed curve). This is because the lower order modes have larger frequency shifts than the higher order modes so that energy is nonuniformly shifted across frequency. The phase of the demodulated time series in Fig. 7(b) shows that the phase angle versus time for the stationary target (dashed curve) varies slowly but is no longer nearly a constant like in free space and for a silt bottom. This is because of the higher order modes introduce different phase changes. The phase change versus time (solid curve) is not changing at a constant rate as in free space or for a silt bottom. The higher order modes introduce multiple Doppler shifts and alter the rate of phase change. Figure 7(c) shows the scaled phase rate $\mu(t)$ of the demodulated time series calculated by Eq. (65). The dashed curve is for the stationary target and the solid curve is for the moving target. The strong late arrivals in the received field shown in Fig. 7(a) introduce significant distortion of the phase angle in Fig. 7(b) and make the scaled

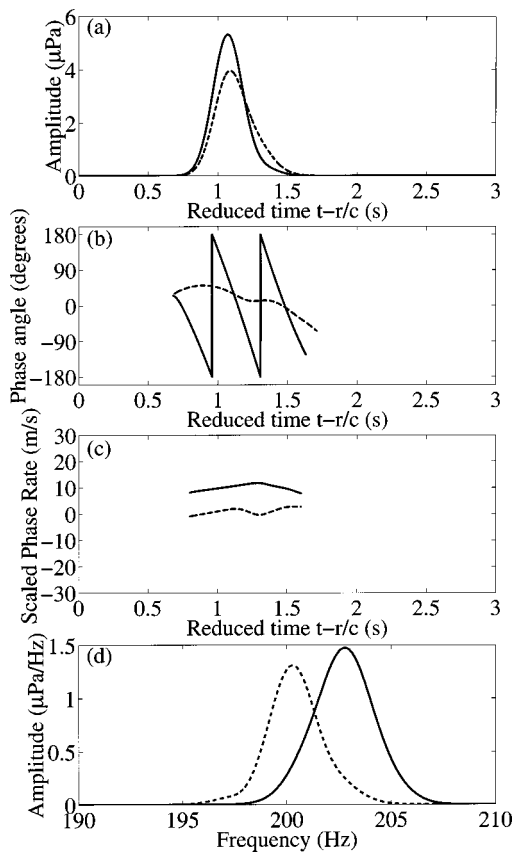


FIG. 11. Same as Fig. 6 except the bottom type is sand and the target is at 3000 m horizontal range from source/receiver.

phase rates in Fig. 7(c) inconsistent with the target's true radial velocities. Even if the target is not moving at all, a rapid change occurs in the scaled phase rate when a strong late arrival corresponding to a higher order mode with slower group velocity arrives. The difference between the scaled phase rate $\mu(t)$ and the target's true radial velocity can be greater than 10 m/s when a strong late arrival is received. This example shows that when the sonar return is significantly distorted by multimodal effects, the scaled phase rate $\mu(t)$ in Eq. (65) cannot be used to reliably estimate the target's radial component velocity.

Limestone bottoms typically have relatively low attenuation, support many higher order modes and so lead to highly dispersive shallow water propagation. As shown in the received field scattered by a stationary sphere (dashed curves) and by a sphere moving at 10 m/s toward the source (solid curves) in Fig. 8(a), several late arrivals are present with long time delays induced by the higher order modes. The highly distorted spectra for a stationary sphere and a sphere moving toward the source at 10 m/s are shown in Fig. 8(d). Again, the Doppler-shifted frequency spectrum (solid curve) is not simply a translated version of the stationary spectrum (dashed curve). Figure 8(b) shows that the phase changes significantly versus time due to the multimodal effects even if the target is not moving. While the target is moving, the phase change is complicated due to the multiple Doppler shifts. The scaled phase rate $\mu(t)$ of the demodulated time series in Eq. (65) for both the stationary and moving target are shown as the dashed curve and the solid curve in Fig.

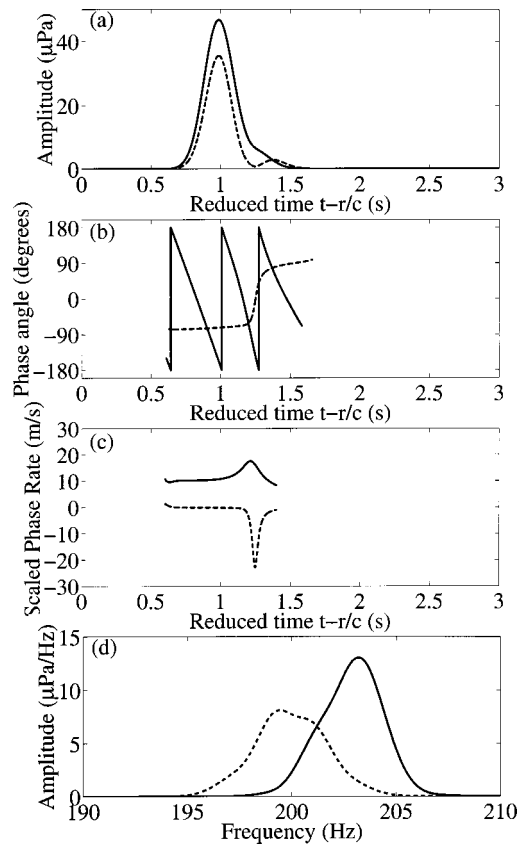


FIG. 12. Same as Fig. 6 except the bottom type is sand and the target is a perfectly reflective disk with $ka = 12$ at 200 Hz.

8(c). As in the waveguide with a sand bottom, rapid changes of scaled phase rate occur making it differ by more than 10 m/s from the true value of the target's radial velocity. All these results indicate that the Doppler shifts in the scattered field are highly dependent on the ocean environment.

Since Doppler effects are a function of target velocity, target velocity may be estimated by measurements of Doppler shifted fields given a known source function and waveguide environment. The sensitivity of the Doppler shifted field to variations in target velocity then becomes an important factor. To investigate this issue, consider again the case of a sand bottom with a spherical target as in Fig. 7, but now with the target moving toward the source at 5 m/s rather than 10 m/s. Figure 9 shows the time series and spectrum of the resulting scattered field, where the solid curve in Fig. 9(d) is the Doppler shifted spectrum. As expected, the dispersive effect in the time series and the frequency shift in the spectrum is smaller for reduced target speed. The phase of the demodulated time series for the target moving at 5 m/s also changes slower than when the target is moving at 10 m/s as shown in Fig. 9(b). These effects are significant since the reduction in time spread of the higher order modes is on the order of tenths of a second and the frequency spectrum is significantly altered over the entire bandwidth of the signal. When the target is moving away from the source, the Doppler frequency shifts are negative. To illustrate this, Fig. 10 shows the time series and spectra for the scattered field from a sphere moving away from the source at 10 m/s, where the bottom type is sand as in Fig. 7. The first arrival for the

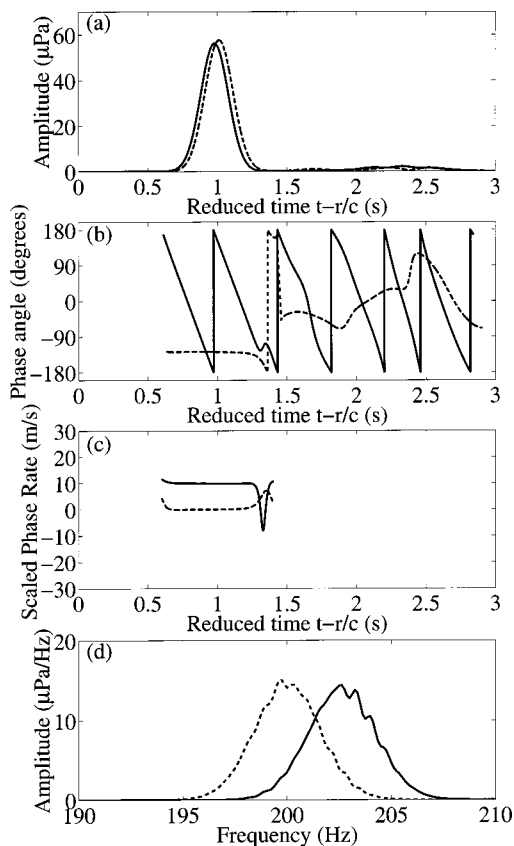


FIG. 13. Same as Fig. 12 except the bottom type is limestone.

moving target in Fig. 10(a) arrives slightly later than in the stationary case because the target is moving away from the source. The negative frequency shift is significant, and on the order of the signal bandwidth, as is evident in the spectrum in Fig. 10(d). The negative frequency shift is also shown as the positive rate of phase change of the solid curve in Fig. 10(b). On the other hand, the rate of phase change is negative for a target moving toward the source and receiver.

The next example illustrates Doppler effects at greater target ranges. Using sand as the bottom type and the sphere at 3000 m initial range from the source, the time series [dashed curves in Fig. 11(a)] is dispersed less than the dashed curves in Fig. 7(a) where the horizontal range is 2000 m. The scattered field from a target moving toward the source at 10 m/s [solid curves in Fig. 11(a)] is also dispersed less than those in Fig. 7(a). This indicates that Doppler effects are highly dependent on the measured geometry.

A perfectly reflecting circular disk facing the source with the same radius as the sphere of $ka=12$ at 200 Hz is used to illustrate variations in the scattered field for flat versus rounded targets. A sand bottom as used in Fig. 7 is also used in Fig. 12. Figures 12(a), 12(b), and 12(d) show the scattered field from a stationary disk and a disk moving toward the source at 10 m/s. With the same measurement geometry and 2000 m as the initial horizontal distance, the time series in Fig. 12(a) appear to be dispersed far less than the time series in Fig. 7(a). The unshifted and shifted frequency spectra of Fig. 12(d) also exhibit this phenomenon. The same measurement geometry and scatterer is used in Fig. 13 but with a limestone bottom. Figures 13(a) and 13(b) show the

scattered field from a stationary disk and a disk moving toward the source at 10 m/s. These time series are also much less dispersive than the scattered field from a spherical scatterer. The unshifted and shifted frequency spectra in Fig. 13(d) are both less distorted than the spectra with a spherical scatterer in Fig. 8(d). This is because scattering from the disk is much stronger in the specular direction than the other directions. Figure 3(b) shows the magnitude of the free-space plane-wave scattering function of the circular disk. Comparing Figs. 3(a) and (b), we can see that the scattering function of the sphere does not vary too much near the specular reflection direction. This leads to relatively uniform coupling between different modes of the incident and scattered field. On the other hand, the disk is highly directional near the specular reflection direction and gives strongest coupling between a given mode of the incident field and the same mode of the scattered field, i.e., diagonal terms of a coupling matrix. Since higher order modes attenuate more than lower order modes and the coupling term between a lower order mode and a higher order mode is weaker, the received signal is dominated by the lower order modes of both the incident and scattered field from the disk. Time-frequency spreading is also significantly weaker than for a spherical scatterer.

It is not always true that the scattered field is stronger when the target is moving toward the source than at rest in a waveguide. For a moving source in free space, the sound field in the forward direction is always more intense than that in the back direction because of the factor $[1 - M \cos \theta]^{-1}$ in pressure, which accounts for free-space dynamics, where M is the Mach number and θ is the angle between the direction of motion and the direction of the field point.² In a waveguide, although there are similar dynamical factors

$$\left[1 + \frac{v_0}{v_l^G(\Omega)} \cos(\phi_0^0 - \varphi_0) \right]^{-1},$$

$$\left[1 - \frac{v_\sigma}{v_m^G(\omega_{m,l})} \cos(\phi^0 - \varphi_\sigma) \right]^{-1}$$

in the modal expression of Eq. (59), they are so close to unity for low Mach number motions of the source and target, respectively, and are not the dominant factors for the changes of signal amplitudes. In a waveguide the field magnitude can fluctuate rapidly as a function of position, frequency, and waveguide environment due to modal interference. The observed fluctuations in field magnitude of the various examples given are dominated by such changes in modal interference as a function of frequency due to Doppler shifting. For example, Fig. 6(d) shows that with a silt bottom and a target moving toward the source, the scattered field is actually weaker than the scattered field from a stationary target because the modal interference with Doppler shifting is more destructive than without.

IV. CONCLUSION

Analytical expressions for the three-dimensional field scattered by a moving target from a moving source to a moving receiver in a general horizontally stratified ocean waveguide are derived from first principles using the time-domain

formulation of Green's theorem. Spectral and modal representations of the Doppler-shifted scattered field for a simple harmonic source and a source with arbitrary time dependence are obtained. The expressions are valid when the source and receiver are sufficiently far from the target that multiple scattering between the target and waveguide boundaries can be neglected and the scattered field can be expressed as a linear function of the target's plane wave scattering function. The source, target, and receiver are assumed to move horizontally with low Mach numbers, as is typical in many active sonar scenarios.

The modal representation has a compelling physical interpretation exhibited by the fact that a simple harmonic source that excites N modes in the waveguide, for example, will excite roughly N^2 distinct harmonic components in the scattered field due to coupling between the incident modes and the scattered modes. The spectral representation, however, is more general and can be used at closer ranges to the target.

Simulations show that Doppler shifts induced in the scattered field by target motion are highly dependent on the waveguide environment, target shape, and measurement geometry. For a highly dispersive waveguide that supports many trapped modes, the frequency spectrum of the field scattered by a moving target typically exhibits significant distortion compared to that of a stationary target or the same target moving in free space. Rounded scatterers with relatively omnidirectional scattering functions, such as spherical scatterers, have greater coupling between incident modes and scattered modes than flat objects that scatter strongest in the specular direction. The scattered field from an object in a multimodal waveguide tends to suffer greater dispersion as the target becomes more rounded and the scattering becomes more omnidirectional.

It is noteworthy that when the target, source, or receiver are moving, the scattered field no longer obeys reciprocity, as is evident in our present formulation. The concept of a time-reversal mirror⁹⁻¹¹ therefore is not directly applicable under motion of the target, source, or receiver. This is true in both free space and in a stratified medium.

A new derivation for the Doppler shifted field radiated to a moving receiver from a moving source in a stratified medium that proved advantageous in the present work is also presented. The new modal formulation is more accurate than previous formulations, since for example, it accounts for variation in mode shape due to Doppler shift.

APPENDIX A: SPECTRAL REPRESENTATION OF THE DOPPLER-SHIFTED FIELD RADIATED BY A MOVING SOURCE TO A MOVING RECEIVER IN A STRATIFIED WAVEGUIDE

A spectral representation for the wave field induced by a moving source and measured at a moving receiver has been presented in Ref. 4. An alternative derivation utilizing Eq. (5) is presented here to represent incident fields in the scattering problem. The result is consistent with prior research but is better suited to the problem at hand.

The location of a moving source is denoted by

$$\mathbf{r}_0 = \mathbf{r}_0^0 + \mathbf{v}_0 t_0, \quad (\text{A1})$$

where \mathbf{r}_0^0 is the initial location of the source at $t_0=0$ and \mathbf{v}_0 is its horizontal velocity. For simple-harmonic radiation at frequency Ω , the source function $q(\mathbf{r}_s, t_0)$ is

$$q(\mathbf{r}_s, t_0) = e^{-i\Omega t_0} \delta(\mathbf{r}_s - \mathbf{r}_0^0 - \mathbf{v}_0 t_0). \quad (\text{A2})$$

The location of a moving receiver is denoted by

$$\mathbf{r} = \mathbf{r}^0 + \mathbf{v} t, \quad (\text{A3})$$

where \mathbf{r}^0 is the initial location of the receiver at $t=0$ and \mathbf{v} is its horizontal velocity. After changing the variables of integration in Eq. (5) from \mathbf{r}_0 to \mathbf{r}_s and V_0 to V_s , and applying Eq. (A2), Eq. (5) becomes

$$\Phi_i(\mathbf{r}, t) = \int_0^{t^+} dt_0 G((\mathbf{r}^0 + \mathbf{v} t), t | (\mathbf{r}_0^0 + \mathbf{v}_0 t_0), t_0) e^{-i\Omega t_0}. \quad (\text{A4})$$

Green's function for the time-domain scalar wave equation of the waveguide can be obtained by applying an inverse Fourier transform to Green's function for the Helmholtz equation at frequency ω ,

$$G(\mathbf{r}, t | \mathbf{r}_0, t_0) = \frac{1}{2\pi} \int_{-\infty}^{\infty} G(\mathbf{r} | \mathbf{r}_0; \omega) e^{-i\omega(t-t_0)} d\omega, \quad (\text{A5})$$

where the spectral representation of Green's function for the Helmholtz equation of a stratified waveguide is given by

$$G(\mathbf{r} | \mathbf{r}_0; \omega) = \frac{1}{2\pi} \int_{-\infty}^{\infty} d^2 \xi_i g(z, z_0; \omega) e^{i\xi_i \cdot (\boldsymbol{\rho} - \boldsymbol{\rho}_0)}. \quad (\text{A6})$$

The depth dependent Green function $g(z, z_0; \omega)$ in Eq. (A6) is defined as

$$g(z, z_0; \omega) = \frac{1}{2\pi} \int_{-\infty}^{\infty} d^2 \boldsymbol{\rho}' G(\mathbf{r} | \mathbf{r}_0; \omega) e^{-i\xi_i \cdot \boldsymbol{\rho}'}, \quad (\text{A7})$$

where $\boldsymbol{\rho}' = \boldsymbol{\rho} - \boldsymbol{\rho}_0$. With this Eq. (A5) can be expressed as

$$G(\mathbf{r}, t | \mathbf{r}_0, t_0) = \frac{1}{2\pi} \int_{-\infty}^{\infty} d\omega e^{-i\omega(t-t_0)} \times \frac{1}{2\pi} \int_{-\infty}^{\infty} d^2 \xi_i g(z, z_0; \omega) e^{i\xi_i \cdot (\boldsymbol{\rho} - \boldsymbol{\rho}_0)}. \quad (\text{A8})$$

After inserting Eq. (A8) into Eq. (A4), the incident field becomes

$$\Phi_i(\mathbf{r}, t) = \frac{1}{2\pi} \int_0^{t^+} dt_0 \frac{1}{2\pi} \int_{-\infty}^{\infty} d\omega e^{-i\omega t} e^{i(\omega - \Omega)t_0} \times \int_{-\infty}^{\infty} d^2 \xi_i g(z, z_0; \omega) e^{i\xi_i \cdot (\boldsymbol{\rho}^0 + \mathbf{v} t - \boldsymbol{\rho}_0^0 - \mathbf{v}_0 t_0)}. \quad (\text{A9})$$

For sufficiently long duration t , integration over t_0 leads to

$$\begin{aligned}
\Phi_i(\mathbf{r}, t) &= \frac{1}{2\pi} \int_{-\infty}^{\infty} d\omega e^{-i\omega t} \int_{-\infty}^{\infty} d^2\xi_i \delta(\omega - \Omega - \xi_i \cdot \mathbf{v}_0) \\
&\quad \times g(z, z_0; \omega) e^{i\xi_i \cdot (\boldsymbol{\rho}^0 + \mathbf{v}t - \boldsymbol{\rho}_0^0)} \\
&= \frac{1}{2\pi} \int_{-\infty}^{\infty} d^2\xi_i g(z, z_0; \Omega + \xi_i \cdot \mathbf{v}_0) \\
&\quad \times e^{i\xi_i \cdot [\boldsymbol{\rho}^0 - \boldsymbol{\rho}_0^0]} e^{-i(\Omega + \xi_i \cdot (\mathbf{v}_0 - \mathbf{v}))t}, \tag{A10}
\end{aligned}$$

which is consistent with Eq. (14) of Ref. 4.

APPENDIX B: NORMAL MODE REPRESENTATION OF THE DOPPLER-SHIFTED FIELD RADIATED BY A MOVING SOURCE TO A MOVING RECEIVER IN A STRATIFIED WAVEGUIDE

The incident field from a moving source at a moving receiver is derived with an alternative modal method and compared with prior results of Ref. 3.

Green's function for the Helmholtz equation of the waveguide can be expressed in terms of normal modes by

$$\begin{aligned}
G(\mathbf{r}_\sigma | \mathbf{r}_0; \omega) &= \frac{id}{4} \sum_l u_l(z_\sigma; \omega) u_l(z_0; \omega) H_0^{(1)}(\xi_l(\omega) |\boldsymbol{\rho}_\sigma - \boldsymbol{\rho}_0|) \\
&\approx \frac{id}{\sqrt{8\pi}} e^{-i(\pi/4)} \sum_l \frac{u_l(z_\sigma; \omega) u_l(z_0; \omega)}{\sqrt{\xi_l(\omega) |\boldsymbol{\rho}_\sigma - \boldsymbol{\rho}_0|}} \\
&\quad \times e^{i\xi_l(\omega) |\boldsymbol{\rho}_0 - \boldsymbol{\rho}_\sigma|}. \tag{B1}
\end{aligned}$$

We take the receiver $\boldsymbol{\rho}_\sigma$ to be a point on the target for consistency with the derivation of the target scattering problem. For a moving target, the horizontal position vector $\boldsymbol{\rho}_\sigma$ of a point on the target is

$$\begin{aligned}
\boldsymbol{\rho}_\sigma &= \boldsymbol{\rho}_\sigma^0 + \mathbf{v}_\sigma t_\sigma \\
&= (\rho_\sigma^0 \cos \phi_\sigma^0 \mathbf{i}_x + \rho_\sigma^0 \sin \phi_\sigma^0 \mathbf{i}_y) \\
&\quad + (v_\sigma t_\sigma \cos \varphi_\sigma \mathbf{i}_x + v_\sigma t_\sigma \sin \varphi_\sigma \mathbf{i}_y), \tag{B2}
\end{aligned}$$

where $\boldsymbol{\rho}_\sigma^0$ is the initial horizontal position at $t_\sigma=0$ and \mathbf{v}_σ is the horizontal velocity of the target point. Similarly, the horizontal position vector of the moving source $\boldsymbol{\rho}_0$ is

$$\begin{aligned}
\boldsymbol{\rho}_0 &= \boldsymbol{\rho}_0^0 + \mathbf{v}_0 t_0 \\
&= (\rho_0^0 \cos \phi_0^0 \mathbf{i}_x + \rho_0^0 \sin \phi_0^0 \mathbf{i}_y) \\
&\quad + (v_0 t_0 \cos \varphi_0 \mathbf{i}_x + v_0 t_0 \sin \varphi_0 \mathbf{i}_y), \tag{B3}
\end{aligned}$$

where $\boldsymbol{\rho}_0^0$ is the initial horizontal position at $t_0=0$ and \mathbf{v}_0 is its horizontal velocity of the source.

We assume the horizontal range ρ_0 of the source is much larger than the range to the target point ρ_σ . In the present formulation, the displacements due to motion are assumed to be much smaller than ρ_0 . This is typically a good assumption for low Mach number motions of the source and target even after they have been operating after many periods of the simple-harmonic source, i.e., $t_0, t_\sigma \gg 2\pi/\Omega$. Therefore, the azimuthal angles of the vectors $\boldsymbol{\rho}_0^0 + \mathbf{v}_0 t_0 - \boldsymbol{\rho}_\sigma^0$ and $\boldsymbol{\rho}_0^0 - \boldsymbol{\rho}_\sigma^0$ are approximately the same. An approximation can then be made

$$\begin{aligned}
|\boldsymbol{\rho}_0 - \boldsymbol{\rho}_\sigma| &\approx \rho_0^0 - \rho_\sigma^0 \cos(\phi_0^0 - \phi_\sigma^0) + v_0 t_0 \cos(\phi_0^0 - \varphi_0) \\
&\quad - v_\sigma t_\sigma \cos(\phi_0^0 - \varphi_\sigma), \tag{B4}
\end{aligned}$$

as in Eq. (44c). After substituting these expressions in Eq. (A5), Green's function for the time domain wave equation of the waveguide becomes

$$\begin{aligned}
G(\mathbf{r}_\sigma, t_\sigma | \mathbf{r}_0, t_0) &= \frac{1}{2\pi} \int_{-\infty}^{\infty} d\omega e^{-i\omega(t_\sigma - t_0)} \frac{id}{\sqrt{8\pi}} e^{-i(\pi/4)} \\
&\quad \times \sum_l \frac{u_l(z_\sigma; \omega) u_l(z_0; \omega)}{\sqrt{\xi_l(\omega) \rho_0^0}} \\
&\quad \times e^{i\xi_l(\omega) [\rho_0^0 - \rho_\sigma^0 \cos(\phi_0^0 - \phi_\sigma^0)]} e^{i\xi_l(\omega) v_0 \cos(\phi_0^0 - \varphi_0) t_0} \\
&\quad \times e^{-i\xi_l(\omega) v_\sigma \cos(\phi_0^0 - \varphi_\sigma) t_\sigma}. \tag{B5}
\end{aligned}$$

Similarly, the incident field in Eq. (A4) becomes

$$\begin{aligned}
\Phi_i(\mathbf{r}_\sigma, t_\sigma) &= \frac{1}{2\pi} \int_0^{t_\sigma^+} dt_0 \int_{-\infty}^{\infty} d\omega e^{-i\omega t_\sigma} e^{i(\omega - \Omega)t_0} \\
&\quad \times \frac{id}{\sqrt{8\pi}} e^{-i(\pi/4)} \sum_l \frac{u_l(z_\sigma; \omega) u_l(z_0; \omega)}{\sqrt{\xi_l(\omega) \rho_0^0}} \\
&\quad \times e^{i\xi_l(\omega) [\rho_0^0 - \rho_\sigma^0 \cos(\phi_0^0 - \phi_\sigma^0)]} \\
&\quad \times e^{i\xi_l(\omega) v_0 \cos(\phi_0^0 - \varphi_0) t_0} \\
&\quad \times e^{-i\xi_l(\omega) v_\sigma \cos(\phi_0^0 - \varphi_\sigma) t_\sigma}. \tag{B6}
\end{aligned}$$

For sufficiently long time duration t_σ , the integral over t_0 can be approximated as

$$\begin{aligned}
\Phi_i(\mathbf{r}_\sigma, t_\sigma) &= \int_{-\infty}^{\infty} d\omega e^{-i\omega t_\sigma} \frac{id}{\sqrt{8\pi}} e^{-i(\pi/4)} \\
&\quad \times \sum_l \delta(\omega - \Omega + \xi_l(\omega) v_0 \cos(\phi_0^0 - \varphi_0)) \\
&\quad \times \frac{u_l(z_\sigma; \omega) u_l(z_0; \omega)}{\sqrt{\xi_l(\omega) \rho_0^0}} \\
&\quad \times e^{i\xi_l(\omega) [\rho_0^0 - \rho_\sigma^0 \cos(\phi_0^0 - \phi_\sigma^0)]} \\
&\quad \times e^{-i\xi_l(\omega) v_\sigma \cos(\phi_0^0 - \varphi_\sigma) t_\sigma}. \tag{B7}
\end{aligned}$$

In order to integrate over ω , we need to find the value of ω that makes the argument of the δ function zero. It is a transcendental equation in ω that cannot be solved analytically

$$h(\omega) = \omega - \Omega + \xi_l(\omega) v_0 \cos(\phi_0^0 - \varphi_0) = 0. \tag{B8}$$

Taking the derivative of $h(\omega)$ with respect to ω yields

$$\begin{aligned}
\frac{dh(\omega)}{d\omega} &= 1 + \frac{d\xi_l(\omega)}{d\omega} v_0 \cos(\phi_0^0 - \varphi_0) \\
&= 1 + \frac{v_0}{v_l^G(\omega)} \cos(\phi_0^0 - \varphi_0), \tag{B9}
\end{aligned}$$

where $v_l^G(\omega)$ is the group velocity of the l th mode at frequency ω . For low Mach number motion of the source, the term

$$\frac{v_0}{v_l^G(\omega)} \cos(\phi_0^0 - \varphi_0)$$

is much smaller than unity. Therefore, the change of slope of $h(\omega)$ is small for a small change of ω and the Newton–Raphson method with only a single iteration gives a reasonably accurate solution for Eq. (B8). Using the source frequency Ω as the initial guess, the first iteration of Newton–Raphson method yields

$$\omega_l = \Omega - \frac{h(\Omega)}{h'(\Omega)} = \Omega - \frac{\xi_l(\Omega) v_0 \cos(\phi_0^0 - \varphi_0)}{1 + \frac{v_0}{v_l^G(\Omega)} \cos(\phi_0^0 - \varphi_0)}. \quad (\text{B10})$$

The horizontal wave number ξ_l and the group velocity v_l^G of the l th mode are both easily evaluated at the source frequency Ω . With the property of the δ function in Eq. (57), the incident field in Eq. (B7) becomes

$$\begin{aligned} \Phi_i(\mathbf{r}_\sigma, t_\sigma) &= \frac{id}{\sqrt{8\pi}} e^{-i(\pi/4)} \sum_l \frac{1}{1 + \frac{v_0}{v_l^G(\Omega)} \cos(\phi_0^0 - \varphi_0)} \\ &\times \frac{u_l(z_\sigma; \omega_l) u_l(z_0; \omega_l)}{\sqrt{\xi_l(\omega_l) \rho_0^0}} \\ &\times e^{i\xi_l(\omega_l)[\rho_0^0 - \rho_\sigma^0 \cos(\phi_0^0 - \phi_\sigma^0)]} \\ &\times e^{-i[\omega_l + \xi_l(\omega_l) v_\sigma \cos(\phi_0^0 - \varphi_\sigma)] t_\sigma}. \quad (\text{B11}) \end{aligned}$$

This expression accounts for the changes in mode shape due to Doppler shifts in frequency that were not considered in Ref. 3. An additional amplification factor

$$\left[1 + \frac{v_0}{v_l^G(\Omega)} \cos(\phi_0^0 - \varphi_0) \right]^{-1}$$

arises that is similar to the $[1 - (v_0/c) \cos \theta]^{-1}$ factor for the field induced by a moving source in free space as discussed in Refs. 1 and 2 and shown in Eq. (C18).

Our result is consistent with Eq. (35) of Ref. 3 to first order. The major difference is that all terms in the formulation of Ref. 3 are evaluated at the source frequency Ω , but several terms in our formulation are evaluated at the Doppler shifted frequencies. For example, changes in mode shape due to Doppler shifts in frequency are taken into account in our formulation but not in that of Ref. 3. The additional accuracy of the current formulation requires computation of normal modes at shifted frequency components.

APPENDIX C: DERIVATION OF THE PLANE-WAVE SCATTERING FUNCTION FOR A MOVING SCATTERER IN FREE SPACE FROM GREEN'S THEOREM

The purpose here is to derive a surface-integral expression for the plane-wave scattering function of an object moving in free space at low Mach number.

The scattering of plane incident waves from a target moving in free space can be formulated using Green's theorem for the time-domain scalar wave equation, described in Eq. (12).

The location of a point on the surface of the target is denoted by

$$\mathbf{r}_\sigma = \mathbf{r}_c + \mathbf{r}_\sigma^0, \quad (\text{C1})$$

where \mathbf{r}_c is the centroid of the object with elevation angle θ_c and azimuthal angle ϕ_c . The surface point \mathbf{r}_σ relative to \mathbf{r}_c is denoted by the relative position vector \mathbf{r}_σ^0 with elevation angle θ_σ^0 and azimuthal angle ϕ_σ^0 with respect to the object's centroid. Since the shape of the object does not change and the motion is assumed to be irrotational, \mathbf{r}_σ^0 , θ_σ^0 , and ϕ_σ^0 are all independent of time. By defining the cosine between directions (α, β) and (θ, ϕ) as

$$\eta(\alpha, \beta; \theta, \phi) = \cos \alpha \cos \theta + \sin \alpha \sin \theta \cos(\beta - \phi) \quad (\text{C2})$$

an incident plane wave with unit amplitude and frequency ω_i can be expressed as

$$\begin{aligned} \hat{\Phi}_i(\mathbf{r}_\sigma, t_\sigma) &= e^{i[\mathbf{k}_i \cdot \mathbf{r}_\sigma - \omega_i t_\sigma]} \\ &= e^{i[\mathbf{k}_i \cdot (\mathbf{r}_c + \mathbf{r}_\sigma^0) - \omega_i t_\sigma]} \\ &= e^{i\mathbf{k}_i \cdot \mathbf{r}_c} e^{ik_i r_\sigma^0} \eta(\alpha_i, \beta_i; \theta_\sigma^0, \phi_\sigma^0) e^{-i\omega_i t_\sigma}, \quad (\text{C3}) \end{aligned}$$

where $k_i = \omega_i/c$. Green's function in free space can be represented by an inverse Fourier transform of Green's function for the Helmholtz equation via

$$G(\mathbf{r}, t | \mathbf{r}_\sigma, t_\sigma) = \frac{1}{2\pi} \int_{-\infty}^{\infty} G(\mathbf{r} | \mathbf{r}_\sigma; \omega) e^{-i\omega(t-t_\sigma)} d\omega, \quad (\text{C4})$$

where Green's function for the Helmholtz equation is

$$G(\mathbf{r} | \mathbf{r}_\sigma; \omega) = \frac{1}{4\pi} \frac{e^{ik|\mathbf{r} - \mathbf{r}_\sigma|}}{|\mathbf{r} - \mathbf{r}_\sigma|} = \frac{1}{4\pi} \frac{e^{ik|\mathbf{r} - \mathbf{r}_c - \mathbf{r}_\sigma^0|}}{|\mathbf{r} - \mathbf{r}_c - \mathbf{r}_\sigma^0|}$$

with $k = \omega/c$. In the far field where $r \gg r_c$ and $r \gg r_\sigma^0$, Green's function for the Helmholtz equation can be approximated as

$$\begin{aligned} G(\mathbf{r} | \mathbf{r}_\sigma; \omega) &\approx \frac{1}{4\pi r} e^{ikr} e^{-ikr_c \eta(\theta, \phi; \theta_c, \phi_c)} \\ &\times e^{-ikr_\sigma^0 \eta(\theta, \phi; \theta_\sigma^0, \phi_\sigma^0)}. \quad (\text{C5}) \end{aligned}$$

Inserting Eq. (C5) into Eq. (C4) yields

$$\begin{aligned} G(\mathbf{r}, t | \mathbf{r}_\sigma, t_\sigma) &= \frac{1}{2\pi} \frac{1}{4\pi r} \int_{-\infty}^{\infty} e^{ikr} e^{-ikr_c \eta(\theta, \phi; \theta_c, \phi_c)} \\ &\times e^{-ikr_\sigma^0 \eta(\theta, \phi; \theta_\sigma^0, \phi_\sigma^0)} e^{-i\omega(t-t_\sigma)} d\omega. \quad (\text{C6}) \end{aligned}$$

Substituting Eq. (C6) into Eq. (12), the scattered field becomes

$$\begin{aligned}\hat{\Phi}_s(\mathbf{r}, t) = & -\frac{1}{4\pi} \int_0^{t^+} dt_\sigma \frac{1}{2\pi} \int_{-\infty}^{\infty} d\omega \frac{e^{ikr}}{r} e^{-i\omega(t-t_\sigma)} \\ & \times \oint d\mathbf{S}_\sigma \cdot \left([e^{i\mathbf{k}_i \cdot \mathbf{r}_c} e^{ik_i r_\sigma^0} \eta(\alpha_i, \beta_i; \theta_\sigma^0, \phi_\sigma^0)] \right. \\ & \times e^{-i\omega t_\sigma} + \hat{\Phi}_s(\mathbf{r}_\sigma, t_\sigma) \\ & \left. \times \nabla_\sigma [e^{-ikr_c \eta(\theta, \phi; \theta_c, \phi_c)} e^{-ikr_\sigma^0 \eta(\theta, \phi; \theta_\sigma^0, \phi_\sigma^0)}] \right),\end{aligned}\quad (C7)$$

where $\hat{\Phi}_s(\mathbf{r}_\sigma, t_\sigma)$ is the scattered field on the surface of the object induced by an incident plane wave with the wave number vector \mathbf{k}_i and unit amplitude. For low Mach number motions of the target, approximations can be made for the scattered field on the target such that $\hat{\Phi}_s(\mathbf{r}_\sigma, t_\sigma)$ is approximated as the scattered field at the initial location of the surface, with a phase shift factor $e^{i\mathbf{k}_i \cdot \mathbf{r}_c}$ due to rigid translation of the centroid, modulated by $\exp(-i\omega t_\sigma)$ so that

$$\hat{\Phi}_s(\mathbf{r}_\sigma, t_\sigma) \approx \hat{\Phi}_s^0(\mathbf{r}_\sigma, \mathbf{k}_i; \omega_i) e^{-i\omega_i t_\sigma} e^{i\mathbf{k}_i \cdot \mathbf{r}_c}. \quad (C8)$$

If the centroid of the scatterer is moving with constant velocity \mathbf{v}_σ then

$$\mathbf{r}_c = \mathbf{v}_\sigma t_\sigma, \quad (C9)$$

where the initial location of \mathbf{r}_c at $t_\sigma=0$ is the coordinate system's origin. Substituting Eqs. (C8) and (C9) into Eq. (C7) yields

$$\begin{aligned}\hat{\Phi}_s(\mathbf{r}, t) = & -\frac{1}{4\pi} \int_0^{t^+} dt_\sigma \frac{1}{2\pi} \int_{-\infty}^{\infty} d\omega \frac{e^{ikr}}{r} e^{-i\omega(t-t_\sigma)} \\ & \times \oint d\mathbf{S}_\sigma \cdot \left([e^{ik_i r_\sigma^0} \eta(\alpha_i, \beta_i; \theta_\sigma^0, \phi_\sigma^0)] \right. \\ & \times e^{-i(\omega_i - \mathbf{k}_i \cdot \mathbf{v}_\sigma) t_\sigma} + \hat{\Phi}_s^0(\mathbf{r}_\sigma, \mathbf{k}_i; \omega_i) e^{-i(\omega_i - \mathbf{k}_i \cdot \mathbf{v}_\sigma) t_\sigma} \\ & \left. \times \nabla_\sigma [e^{-ikv_\sigma t_\sigma \eta(\theta, \phi; \theta_c, \phi_c)} e^{-ikr_\sigma^0 \eta(\theta, \phi; \theta_\sigma^0, \phi_\sigma^0)}] \right).\end{aligned}\quad (C10)$$

For sufficiently long time duration t , the integral over t_σ introduces the delta function $\delta(\omega(1 - (v_\sigma/c)) \times \eta(\theta, \phi; \theta_c, \phi_c) - \omega_i + \mathbf{k}_i \cdot \mathbf{v}_\sigma)$ to the integrand. The property of the δ function described in Eq. (57) in this case leads to

$$\omega^* = \frac{\omega_i - \mathbf{k}_i \cdot \mathbf{v}_\sigma}{1 - \frac{v_\sigma}{c} \eta(\theta, \phi; \theta_c, \phi_c)}, \quad (C11)$$

where ω^* is the Doppler shifted frequency in the direction of propagation (θ, ϕ) . Integrating over ω then yields

$$\begin{aligned}\hat{\Phi}_s(\mathbf{r}, t) = & -\frac{1}{4\pi} \frac{1}{1 - \frac{v_\sigma}{c} \eta(\theta, \phi; \theta_c, \phi_c)} \frac{e^{i\omega^*((r/c)-t)}}{r} \\ & \times \oint d\mathbf{S}_\sigma \cdot \left([e^{ik_i r_\sigma^0} \eta(\alpha_i, \beta_i; \theta_\sigma^0, \phi_\sigma^0)] + \hat{\Phi}_s^0(\mathbf{r}_\sigma, \mathbf{k}_i; \omega_i) \right. \\ & \left. \times \nabla_\sigma [e^{-i(\omega^*/c)r_\sigma^0} \eta(\theta, \phi; \theta_\sigma^0, \phi_\sigma^0)] \right).\end{aligned}\quad (C12)$$

In the far field, the scattered field can be approximated as a point source radiating with an angular weighting factor¹⁵ given by the object's plane-wave scattering function via

$$\Psi_s(\mathbf{r}|\mathbf{r}_c; \omega) \approx \frac{e^{ik|\mathbf{r}-\mathbf{r}_c|}}{k|\mathbf{r}-\mathbf{r}_c|} S(\theta, \phi; \alpha_i, \beta_i; \omega), \quad (C13)$$

which for $r \gg r_c$ reduces to

$$\begin{aligned}\Psi_s(\mathbf{r}|\mathbf{r}_c; \omega) \approx & \frac{1}{kr} e^{ikr} e^{-ikr_c \eta(\theta, \phi; \theta_c, \phi_c)} \\ & \times S(\theta, \phi; \alpha_i, \beta_i; \omega).\end{aligned}\quad (C14)$$

The field induced by a moving point source can be expressed as

$$\hat{\Phi}_s(\mathbf{r}, t) = \int_0^{t^+} dt_\sigma \int dV_c \Psi_s(\mathbf{r}, t|\mathbf{r}_c, t_\sigma) q(\mathbf{r}_c, t_\sigma) \quad (C15)$$

with source function

$$q(\mathbf{r}_c, t_\sigma) = e^{-i\omega_i t_\sigma} \delta(\mathbf{r}_c - \mathbf{v}_\sigma t_\sigma). \quad (C16)$$

Equation (C15) then becomes

$$\begin{aligned}\hat{\Phi}_s(\mathbf{r}, t) = & \int_0^{t^+} dt_\sigma \frac{1}{2\pi} \int_{-\infty}^{\infty} d\omega e^{-i\omega(t-t_\sigma)} \Psi_s(\mathbf{r}|\mathbf{v}_\sigma t_\sigma; \omega) e^{-i\omega_i t_\sigma} \\ \approx & \int_0^{t^+} dt_\sigma \frac{1}{2\pi} \int_{-\infty}^{\infty} d\omega \frac{e^{ikr}}{r} e^{-i\omega(t-t_\sigma)} \\ & \times \frac{1}{k} S(\theta, \phi; \alpha_i, \beta_i; \omega) e^{-i(\omega_i - \mathbf{k}_i \cdot \mathbf{v}_\sigma) t_\sigma} \\ & \times e^{-ikv_\sigma t_\sigma \eta(\theta, \phi; \theta_c, \phi_c)}.\end{aligned}\quad (C17)$$

Using similar techniques as before to integrate over t_σ and ω , the scattered field becomes

$$\begin{aligned}\hat{\Phi}_s(\mathbf{r}, t) = & \frac{1}{1 - \frac{v_\sigma}{c} \eta(\theta, \phi; \theta_c, \phi_c)} \frac{e^{i\omega^*((r/c)-t)}}{\frac{\omega^*}{c} r} \\ & \times S(\theta, \phi; \alpha_i, \beta_i; \omega^*),\end{aligned}\quad (C18)$$

where $[1 - (v_\sigma/c) \eta(\theta, \phi; \theta_c, \phi_c)]^{-1}$ is a dynamical factor due to the motion.² By equating Eq. (C12) with Eq. (C18), the plane-wave scattering function $S(\theta, \phi; \alpha_i, \beta_i; \omega^*)$ for an object moving at low Mach number in free space can be written in terms of a surface integral over the object by

$$\begin{aligned}S(\theta, \phi; \alpha_i, \beta_i; \omega^*) \approx & -\frac{\omega^*}{4\pi c} \oint d\mathbf{S}_\sigma \cdot ([e^{ik_i r_\sigma^0} \eta(\alpha_i, \beta_i; \theta_\sigma^0, \phi_\sigma^0)] \\ & + \hat{\Phi}_s^0(\mathbf{r}_\sigma, \mathbf{k}_i; \omega_i)] \nabla_\sigma [e^{-i(\omega^*/c)r_\sigma^0} \eta(\theta, \phi; \theta_\sigma^0, \phi_\sigma^0)]).\end{aligned}\quad (C19)$$

If the object is not moving, Eq. (C19) leads to the special case Eq. (C9) of Ref. 6 directly.

APPENDIX D: DERIVATION OF THE NORMAL MODE REPRESENTATION OF THE DOPPLER-SHIFTED FIELD SCATTERED FROM A MOVING TARGET BY A SOURCE WITH ARBITRARY TIME DEPENDENCE IN A STRATIFIED WAVEGUIDE

Using the incident field described in Eq. (B7) and decomposing the field into upgoing and downgoing plane waves yields

$$\begin{aligned} \Phi_i(\mathbf{r}_\sigma, t_\sigma) &= \int_{-\infty}^{\infty} d\omega_0 \sum_I \delta(\omega_0 - \Omega + \xi_I(\omega_0)v_0 \cos(\phi_0^0 - \varphi_0)) \\ &\times [A_I(\mathbf{r}_0^0; \omega_0) e^{ik(\omega_0)r_\sigma^0 \eta(\alpha_I, \pi - \phi_0^0; \theta_\sigma^0, \phi_\sigma^0)} \\ &- B_I(\mathbf{r}_0^0; \omega_0) e^{ik(\omega_0)r_\sigma^0 \eta(\pi - \alpha_I, \pi - \phi_0^0; \theta_\sigma^0, \phi_\sigma^0)}] \\ &\times e^{-i(\omega_0 + \xi_I(\omega_0)v_0 \cos(\phi_0^0 - \varphi_0))t_\sigma}. \end{aligned} \quad (D1)$$

As in Sec. II C the total scattered field on the surface of the target can be represented as

$$\begin{aligned} \Phi_s(\mathbf{r}_\sigma, t_\sigma) &= \int_{-\infty}^{\infty} d\omega_0 \sum_I \delta(\omega_0 - \Omega + \xi_I(\omega_0)v_0 \cos(\phi_0^0 - \varphi_0)) \\ &\times [A_I(\mathbf{r}_0^0; \omega_0) \hat{\Phi}_s(\mathbf{r}_\sigma, \mathbf{k}_I^+; \omega_0) \\ &- B_I(\mathbf{r}_0^0; \omega_0) \hat{\Phi}_s(\mathbf{r}_\sigma, \mathbf{k}_I^-; \omega_0)] \end{aligned}$$

$$- B_I(\mathbf{r}_0^0; \omega_0) \hat{\Phi}_s(\mathbf{r}_\sigma, \mathbf{k}_I^-; \omega_0)] e^{-i\omega_0 t_\sigma}. \quad (D2)$$

For low Mach number motion, $\hat{\Phi}_s(\mathbf{r}_\sigma, \mathbf{k}_I^+; \omega_0)$ and $\hat{\Phi}_s(\mathbf{r}_\sigma, \mathbf{k}_I^-; \omega_0)$ are approximated as the scattered fields at the initial location of the surface $\hat{\Phi}_s(\mathbf{r}_\sigma^0, \mathbf{k}_I^+; \omega_0)$ and $\hat{\Phi}_s(\mathbf{r}_\sigma^0, \mathbf{k}_I^-; \omega_0)$ multiplied by the phase shift $e^{-i\xi_I(\omega_0)v_0 \cos(\phi_0^0 - \varphi_0)t_\sigma}$

Equation (D2) then becomes

$$\begin{aligned} \Phi_s(\mathbf{r}_\sigma, t) &= \int_{-\infty}^{\infty} d\omega_0 \sum_I \delta(\omega_0 - \Omega + \xi_I(\omega_0)v_0 \cos(\phi_0^0 - \varphi_0)) \\ &\times [A_I(\mathbf{r}_0^0; \omega_0) \hat{\Phi}_s(\mathbf{r}_\sigma^0, \mathbf{k}_I^+; \omega_0) \\ &- B_I(\mathbf{r}_0^0; \omega_0) \hat{\Phi}_s(\mathbf{r}_\sigma^0, \mathbf{k}_I^-; \omega_0)] \\ &\times e^{-i(\omega_0 + \xi_I(\omega_0)v_0 \cos(\phi_0^0 - \varphi_0))t_\sigma}. \end{aligned} \quad (D3)$$

Substituting Eqs. (46), (D1) and (D3) into Eq. (12), the scattered field induced by a simple-harmonic source with source frequency Ω is expressed as

$$\begin{aligned} \Phi_s(\mathbf{r}, t) &\approx -\frac{1}{2\pi} \int_0^{t^+} dt_\sigma \oint d\mathbf{S}_\sigma \cdot \left\{ \int_{-\infty}^{\infty} d\omega_0 \sum_I \delta(\omega_0 - \Omega + \xi_I(\omega_0)v_0 \cos(\phi_0^0 - \varphi_0)) e^{-i(\omega_0 + \xi_I(\omega_0)v_0 \cos(\phi_0^0 - \varphi_0))t_\sigma} \right. \\ &\times \left(A_I(\mathbf{r}_0^0; \omega_0) [e^{ik(\omega_0)r_\sigma^0 \eta(\alpha_I, \pi - \phi_0^0; \theta_\sigma^0, \phi_\sigma^0)} + \hat{\Phi}_s(\mathbf{r}_\sigma^0, \mathbf{k}_I^+; \omega_0)] \right. \\ &\left. - B_I(\mathbf{r}_0^0; \omega_0) [e^{ik(\omega_0)r_\sigma^0 \eta(\pi - \alpha_I, \pi - \phi_0^0; \theta_\sigma^0, \phi_\sigma^0)} + \hat{\Phi}_s(\mathbf{r}_\sigma^0, \mathbf{k}_I^-; \omega_0)] \right) \\ &\times \nabla_\sigma \left(\int_{-\infty}^{\infty} d\omega e^{-i\omega(t-t_\sigma)} \sum_m [A_m(\mathbf{r}^0; \omega) e^{-ik(\omega)r_\sigma^0 \eta(\pi - \alpha_m, \phi_0^0; \theta_\sigma^0, \phi_\sigma^0)} - B_m(\mathbf{r}^0; \omega) e^{-ik(\omega)r_\sigma^0 \eta(\alpha_m, \phi_0^0; \theta_\sigma^0, \phi_\sigma^0)}] \right. \\ &\left. \times e^{i\xi_m(\omega)v_0 \cos(\phi_0^0 - \varphi_0)t} e^{-i\xi_m(\omega)v_0 \cos(\phi_0^0 - \varphi_0)t_\sigma} \right) \left. \right\}. \end{aligned} \quad (D4)$$

For an arbitrary source with frequency spectrum $Q(\Omega)$, the normal mode representation of the Doppler-shifted scattered field is formulated by Fourier synthesis

$$\Psi_s(\mathbf{r}, t) = \frac{1}{2\pi} \int_{-\infty}^{\infty} d\Omega Q(\Omega) \Phi_s(\mathbf{r}, t). \quad (D5)$$

er's frame of reference is obtained by applying a Fourier transform to Eq. (D5),

$$\Psi_s(\mathbf{r}, \omega') = \int_{-\infty}^{\infty} dt e^{i\omega' t} \Psi_s(\mathbf{r}, t), \quad (D6)$$

where ω' is the frequency in the receiver frame of reference. Integrating over t leads to

$$\begin{aligned}
\Psi_s(\mathbf{r}, \omega') \approx & -\frac{1}{2\pi} \int_{-\infty}^{\infty} d\Omega \mathcal{Q}(\Omega) \int_0^{t^+} dt_\sigma \oint d\mathbf{S}_\sigma \cdot \left\{ \int_{-\infty}^{\infty} d\omega_0 \sum_l \delta(\omega_0 - \Omega + \xi_l(\omega_0)v_\sigma \cos(\phi_0^0 - \varphi_0)) \right. \\
& \times e^{-i(\omega_0 + \xi_l(\omega_0)v_\sigma \cos(\phi_0^0 - \varphi_0))t_\sigma} \\
& \times \left(A_l(\mathbf{r}_0^0; \omega_0) [e^{ik(\omega_0)r_\sigma^0 \eta(\alpha_l, \pi - \phi_0^0; \theta_\sigma^0, \phi_\sigma^0)} + \hat{\Phi}_s(\mathbf{r}_\sigma^0, \mathbf{k}_l^+; \omega_0)] \right. \\
& \left. - B_l(\mathbf{r}_0^0; \omega_0) [e^{ik(\omega_0)r_\sigma^0 \eta(\pi - \alpha_l, \pi - \phi_0^0; \theta_\sigma^0, \phi_\sigma^0)} + \hat{\Phi}_s(\mathbf{r}_\sigma^0, \mathbf{k}_l^-; \omega_0)] \right) \\
& \times \nabla_\sigma \left(\int_{-\infty}^{\infty} d\omega e^{i\omega t_\sigma} \sum_m [A_m(\mathbf{r}^0; \omega) e^{-ik(\omega)r_\sigma^0 \eta(\pi - \alpha_m, \phi^0; \theta_\sigma^0, \phi_\sigma^0)} - B_m(\mathbf{r}^0; \omega) e^{-ik(\omega)r_\sigma^0 \eta(\alpha_m, \phi^0; \theta_\sigma^0, \phi_\sigma^0)}] \right. \\
& \left. \times e^{-i\xi_m(\omega)v_\sigma \cos(\phi^0 - \varphi_\sigma)t_\sigma} \delta(\omega - \omega' - \xi_m(\omega)v_\sigma \cos(\phi^0 - \varphi)) \right) \left. \right\}. \tag{D7}
\end{aligned}$$

In order to integrate over ω , the roots of the transcendental equation of ω need to be computed

$$h(\omega) = \omega - \omega' - \xi_m(\omega)v_\sigma \cos(\phi^0 - \varphi) = 0. \tag{D8}$$

Newton–Raphson method is used to find the approximated solutions of Eq. (D8). First iteration with ω' as the initial guess gives

$$\omega'_m = \omega' - \frac{-\xi_m(\omega')v_\sigma \cos(\phi^0 - \varphi)}{1 - \frac{v}{v_m^G(\omega')} \cos(\phi^0 - \varphi)}, \tag{D9}$$

where $v_m^G(\omega')$ is the group velocity of the m th mode at frequency ω' .

Integrating over ω yields a δ function of ω_0 . Performing integration over Ω yields

$$\begin{aligned}
\Psi_s(\mathbf{r}, \omega') \approx & -\frac{1}{2\pi} \int_0^{t^+} dt_\sigma \oint d\mathbf{S}_\sigma \cdot \left\{ \int_{-\infty}^{\infty} d\omega_0 \sum_l \mathcal{Q}(\omega_0 + \xi_l(\omega_0)v_\sigma \cos(\phi_0^0 - \varphi_0)) e^{-i(\omega_0 + \xi_l(\omega_0)v_\sigma \cos(\phi_0^0 - \varphi_0))t_\sigma} \right. \\
& \times \left(A_l(\mathbf{r}_0^0; \omega_0) [e^{ik(\omega_0)r_\sigma^0 \eta(\alpha_l, \pi - \phi_0^0; \theta_\sigma^0, \phi_\sigma^0)} + \hat{\Phi}_s(\mathbf{r}_\sigma^0, \mathbf{k}_l^+; \omega_0)] \right. \\
& \left. - B_l(\mathbf{r}_0^0; \omega_0) [e^{ik(\omega_0)r_\sigma^0 \eta(\pi - \alpha_l, \pi - \phi_0^0; \theta_\sigma^0, \phi_\sigma^0)} + \hat{\Phi}_s(\mathbf{r}_\sigma^0, \mathbf{k}_l^-; \omega_0)] \right) \\
& \times \nabla_\sigma \left(\sum_m \frac{1}{1 - [v/v_m^G(\omega'_m)] \cos(\phi^0 - \varphi)} [A_m(\mathbf{r}^0; \omega'_m) e^{-ik(\omega'_m)r_\sigma^0 \eta(\pi - \alpha_m, \phi^0; \theta_\sigma^0, \phi_\sigma^0)} \right. \\
& \left. - B_m(\mathbf{r}^0; \omega'_m) e^{-ik(\omega'_m)r_\sigma^0 \eta(\alpha_m, \phi^0; \theta_\sigma^0, \phi_\sigma^0)}] e^{i[\omega'_m - \xi_m(\omega'_m)v_\sigma \cos(\phi^0 - \varphi_\sigma)]t_\sigma} \right) \left. \right\}. \tag{D10}
\end{aligned}$$

For sufficiently long time duration t , the integration over t_σ introduces the delta function $\delta(\omega_0 - \omega'_m + \xi_l(\omega_0)v_\sigma \cos(\phi_0^0 - \varphi_\sigma) + \xi_m(\omega'_m)v_\sigma \cos(\phi^0 - \varphi_\sigma))$ to the integrand. Once again, a transcendental equation in ω_0 for the argument of the delta function needs to be solved by means of Newton–Raphson method

$$h(\omega_0) = \omega_0 - \omega'_m + \xi_l(\omega_0)v_\sigma \cos(\phi_0^0 - \varphi_\sigma) + \xi_m(\omega'_m)v_\sigma \cos(\phi^0 - \varphi_\sigma) = 0. \tag{D11}$$

The derivative of $h(\omega)$ with respect to ω_0 is

$$\frac{dh(\omega_0)}{d\omega_0} = 1 + \frac{v_\sigma}{v_l^G(\omega_0)} \cos(\phi_0^0 - \varphi_\sigma). \tag{D12}$$

First iteration of Newton–Raphson method with ω'_m as the initial guess is

$$\begin{aligned}
\omega'_{l,m} &= \omega'_m - \frac{h(\omega'_m)}{h'(\omega'_m)} \\
&= \omega'_m - \frac{\xi_l(\omega'_m)v_\sigma \cos(\phi_0^0 - \varphi_\sigma) + \xi_m(\omega'_m)v_\sigma \cos(\phi^0 - \varphi_\sigma)}{1 + \frac{v_\sigma}{v_l^G(\omega'_m)} \cos(\phi_0^0 - \varphi_\sigma)}.
\end{aligned} \tag{D13}$$

Integrating over ω_0 finally yields

$$\begin{aligned}
\Psi_s(\mathbf{r}, \omega') &\approx - \oint d\mathbf{S}_\sigma \cdot \left\{ \sum_l \sum_m \mathcal{Q}(\omega'_{l,m} + \xi_l(\omega'_{l,m})v_0 \cos(\phi_0^0 - \varphi_0)) \right. \\
&\quad \times \frac{1}{1 - [v/v_m^G(\omega'_m)] \cos(\phi^0 - \varphi)} \frac{1}{1 + [v_\sigma/v_l^G(\omega'_{l,m})] \cos(\phi_0^0 - \varphi_\sigma)} \\
&\quad \times (A_l(\mathbf{r}_0^0; \omega'_{l,m}) [e^{ik(\omega'_{l,m})r_\sigma^0 \eta(\alpha_l, \pi - \phi_0^0; \theta_\sigma^0, \phi_\sigma^0)} + \hat{\Phi}_s(\mathbf{r}_\sigma^0, \mathbf{k}_l^+; \omega'_{l,m})] \\
&\quad - B_l(\mathbf{r}_0^0; \omega'_{l,m}) [e^{ik(\omega'_{l,m})r_\sigma^0 \eta(\pi - \alpha_l, \pi - \phi_0^0; \theta_\sigma^0, \phi_\sigma^0)} + \hat{\Phi}_s(\mathbf{r}_\sigma^0, \mathbf{k}_l^-; \omega'_{l,m})]) \\
&\quad \left. \times \nabla_\sigma (A_m(\mathbf{r}^0; \omega'_m) e^{-ik(\omega'_m)r_\sigma^0 \eta(\pi - \alpha_m, \phi^0; \theta_\sigma^0, \phi_\sigma^0)} - B_m(\mathbf{r}^0; \omega'_m) e^{-ik(\omega'_m)r_\sigma^0 \eta(\alpha_m, \phi^0; \theta_\sigma^0, \phi_\sigma^0)}) \right\}.
\end{aligned} \tag{D14}$$

¹P. M. Morse and K. U. Ingard, *Theoretical Acoustics* (Princeton University Press, Princeton, NJ, 1968), pp. 721–724.

²A. P. Dowling and J. E. Ffowcs Williams, *Sound and Sources of Sound* (Horwood, Chichester, 1983), pp. 187–199.

³K. E. Hawker, “A normal mode theory of acoustic Doppler effects in the oceanic waveguide,” *J. Acoust. Soc. Am.* **65**, 675–681 (1979).

⁴H. Schmidt and W. A. Kuperman, “Spectral and modal representations of the Doppler-shifted field in ocean waveguides,” *J. Acoust. Soc. Am.* **96**, 386–395 (1994).

⁵N. C. Makris, “A spectral approach to 3-D object scattering in layered media applied to scattering from submerged spheres,” *J. Acoust. Soc. Am.* **104**, 2105–2113 (1998).

⁶F. Ingenito, “Scattering from an object in a stratified medium,” *J. Acoust. Soc. Am.* **82**, 2051–2059 (1987).

⁷N. C. Makris, F. Ingenito, and W. A. Kuperman, “Detection of a submerged object insonified by surface noise in an ocean waveguide,” *J. Acoust. Soc. Am.* **96**, 1703–1724 (1994).

⁸N. C. Makris and P. Ratilal, “A unified model for reverberation and sub-

merged object scattering in a stratified ocean waveguide,” *J. Acoust. Soc. Am.* **109**, 909–941 (2001).

⁹D. R. Jackson and D. R. Dowling, “Phase conjugation in underwater acoustics,” *J. Acoust. Soc. Am.* **89**, 171–181 (1991).

¹⁰M. Fink, “Time-reversed acoustics,” *Phys. Today* **50**, 34–40 (1997).

¹¹H. C. Song, W. A. Kuperman, W. S. Hodgkiss, T. Akal, and C. Ferla, “Interactive time reversal in the ocean,” *J. Acoust. Soc. Am.* **105**, 3176–3184 (1999).

¹²P. M. Morse and H. Feshbach, *Methods of Theoretical Physics* (McGraw–Hill, New York, 1953), Vol. 1, pp. 834–837.

¹³M. B. Porter, The KRAKEN normal mode program, SACLANT Undersea Research Centre, La Spezia, Italy, September, 1991.

¹⁴P. Ratilal, Y. Lai, and N. Makris, “Validity of the sonar equation and Babinet’s principle in a stratified medium,” *J. Acoust. Soc. Am.* **112**, 1797–1816 (2002).

¹⁵*Electromagnetic and Acoustic Scattering by Simple Shapes*, edited by J. J. Bowman, T. B. A. Senior, and P. L. E. Uslenghi (North-Holland, Amsterdam, 1969), p. I.2.